A VPT2 Route to Near-Infrared Spectroscopy: the Role of Mechanical and Electrical Anharmonicity

Julien Bloino*,†,‡

Consiglio Nazionale delle Ricerche, Istituto di Chimica dei Composti OrganoMetallici (ICCOM-CNR), UOS di Pisa, Area della Ricerca CNR, Via G. Moruzzi 1, 56124 Pisa, Italy, and Scuola Normale Superiore, piazza dei Cavalieri 7, I-56126 Pisa, Italy

E-mail: julien.bloino@pi.iccom.cnr.it

*To whom correspondence should be addressed
†CNR-ICCOM
‡Scuola Normale Superiore, piazza dei Cavalieri 7, I-56126 Pisa, Italy

Abstract

Following the previous developments to simulate fully anharmonic spectra within the vibrational second-order perturbation level of theory [J. Chem. Phys 2012, 126, 134108], an extension to transitions up to three quanta is presented here. A general formulation including the mechanical and electrical anharmonicities is adopted in order to facilitate the support of additional properties, and thus spectroscopies. In addition to providing more accurate theoretical band-shapes, inclusion of overtones and combination bands up to three quanta paves the way to a more complete interpretation of near-infrared spectra.

Keywords

Infrared, anharmonicity, intensities, frequencies, overtones

Introduction

Thanks to constant improvements in the models and the efforts devoted to make programs accessible to a wide community of users beyond the field of theoretical chemistry, computational spectroscopy has become a routine tool for the interpretation and prediction of spectra.[1–4] Furthermore, the availability of efficient hardware, even in workstation-like machines, gives the possibility to devise tailored simulations where the accuracy of the models can be balanced with its cost depending on the size and complexity of the molecular systems of interest. In the specific case of vibrational spectroscopy, a remarkable achievement concerns the inclusion of anharmonic effects in the simulations, which can be done through *ad hoc* programs or more general-purpose packages.[5–16] For small molecules, fully variational methods based on an accurate representation of the potential energy surface can be used in order to obtain converged ro-vibrational levels.[11,17–22] However, their high computational cost prevents their feasibility for larger systems and less expensive models are needed, with a

trade-off with respect to the achievable accuracy. Among the alternatives, the most successful ones are those based on the vibrational self-consistent field (VSCF)[23–31] or vibrational second-order perturbation theory (VPT2).[32–44] The latter is particularly appealing since it can reach accurate results at a limited cost, with almost all the computational time due to the generation of the required data and in particular the third and fourth derivatives of the potential energy through numerical differentiation.[45,46] In practice, since each displaced geometry can be treated separately, a significant speedup can be achieved by performing the differentiation along each normal coordinate in parallel.

It should be noted that an alternative way is to compute analytically the cubic and quartic force fields. Such a possibility was first limited to Hartree–Fock,[47–49] but has recently been extended to the density functional theory (DFT) as well thanks to the work of Ruud and coworkers.[50] In the present work, numerical differentiation has been used.

While the calculation of vibrational energies at the VPT2 level is now a routine task widespread in various computational packages, work on transition intensities has been scarcer and either restricted to a type of spectroscopy[51–53] or based on a partial anharmonic treatment, by either considering only the anharmonicity of the wave function (mechanical anharmonicity) or of the property (electric anharmonicity).[53–55] Following the path opened by Handy and coworkers[56] and the derivation proposed by Stanton and Vázquez,[51,57] we have proposed a reformulation of the transition intensities to fundamental bands, overtones and combination bands up to 2 quanta based on a model property, which could be straightforwardly identified to a property of interest, either function of the normal coordinates or their conjugate momenta.[58] This approach has been successfully applied to simulate IR, Raman and VCD spectra of medium-size molecular systems in gas phase and solutions.[59–62] The present work provides an extension to this previous work where transitions to overtones and combination bands up to 3 quanta are explored. This paves the way to the detailed simulation of spectra over a large energy range, well within the near-infrared region (NIR).

This paper is organized as follows. The first part summarizes the principles of the deriva-

tion used to provide general equations for each type of transition and applicable to various properties, such as the electric and magnetic dipoles or the polarizability tensor (both static and frequency-dependent). VPT2 formulas for transition energies and intensities to any excited vibrational state with up to 3 quanta are then derived and gathered in easily implementable forms. As illustrations of the implementations, the IR and NIR spectra of one small system, nitric acid, and two medium-size systems, naphthalene and isobutene, are investigated and analyzed. The supporting information contains simpler formulas obtainable for 3-quanta overtones and 2-states combinations with 1 mode excited with 2 quanta and the other one with 1 quantum, which can be interesting to achieve more efficient implementations.

Theory

Within a time-independent framework, the spectrum band-shape is simulated as a sum of transition between two (theoretically infinite) ensembles of initial and final states, vibrational in the present case. The quantity of interest is chosen to be directly observable experimentally or easily derivable from measurements. Regarding vibrational spectroscopies, infrared (IR), vibrational circular dichroism (VCD) and Raman are commonly given in terms of molar absorption coefficients ($\epsilon(\bar{\nu}_0)$), difference between the molar absorption coefficients ($\Delta\epsilon(\bar{\nu}_0)$) and absolute differential Raman cross sections ($\partial\sigma(\bar{\nu}_0)/\partial\Omega$), respectively,

$$\epsilon(\bar{\nu}_0) = \frac{8\pi^3\mathcal{N}_A\bar{\nu}_0}{3000\ln(10)hc(4\pi\epsilon_0)}\sum_I \rho_I \sum_F D_{IF}\delta(\varepsilon_F - \varepsilon_I - \bar{\nu}_0) \tag{1}$$

$$\Delta\epsilon(\bar{\nu}_0) = \frac{32\pi^3\mathcal{N}_A\bar{\nu}_0}{3000\ln(10)hc^2(4\pi\epsilon_0)}\sum_I \rho_I \sum_F R_{IF}\delta(\varepsilon_F - \varepsilon_I - \bar{\nu}_0) \tag{2}$$

$$\frac{\partial\sigma(\bar{\nu}_0)}{\partial\Omega} = (2\pi)^4\sum_I \rho_I \sum_F (\bar{\nu}_0 - (\varepsilon_F - \varepsilon_I))^4\frac{S_{IF}}{45}\delta(\varepsilon_F - \varepsilon_I - \bar{\nu}_0) \tag{3}$$

where $\bar{\nu}_0$, ε_I and ε_F are the vibrational wavenumbers (in cm^{-1}) of the incident light, and the initial and final states, respectively. ρ_I is the Boltzmann population of state "I" and δ the Dirac function. In practice, the latter is replaced by distribution functions to simulate the broadening observed experimentally. D_{IF}, R_{IF} and S_{IF} are respectively the dipole strength, the rotatory strength and the Raman activity, which will be discussed in detail in the part dedicated to the calculation of the transition intensities. Regarding the units, $\epsilon(\bar{\nu}_0)$ and $\Delta\epsilon(\bar{\nu}_0)$ are commonly expressed in $\mathrm{dm}^3 \cdot \mathrm{mol}^{-1} \cdot \mathrm{cm}^{-1}$, and $\partial\sigma(\bar{\nu}_0)/\partial\Omega$ in $\mathrm{m}^2 \cdot \mathrm{sr}^{-1}$.

In order to get accurate band-shapes, both band positions (vibrational energies) and intensities (transition integrals), must be treated beyond the harmonic approximation. With target molecular systems of medium-to-large sizes, the most suited approach to account for the anharmonic effects is the vibrational second-order perturbation theory (VPT2), which offers a good balance between accuracy and computational cost. In the following, the systems of interest will be assumed devoid of degenerate normal modes (asymmetric tops), so the discussion will be targeted to abelian groups. The case of symmetric and linear molecules will be deferred to a later work.

To conclude this part, as described in the introduction and in Ref.,[58] the inclusion of anharmonicity in the calculation of vibrational energies and intensities has been explored by various groups, which have adopted different approaches and conventions. In order to get a coherent picture, the references used as starting points for the developments have been voluntarily limited to the papers describing the actual implementation used here.

Vibrational energies

The vibrational energies (in cm^{-1}), which are directly related to band positions, can be obtained from a single formula at the VPT2 level. Starting from the implementation described in Ref.,[45] the latter can be written as,

$$\varepsilon_{\boldsymbol{n}} = \chi_0 + \sum_i^N \omega_i \left(n_i + \frac{1}{2}\right) + \sum_i^N \sum_{j=i}^N \chi_{ij} \left(n_i + \frac{1}{2}\right)\left(n_j + \frac{1}{2}\right) \tag{4}$$

where ω_i is the harmonic wavenumber associated to mode i, $\boldsymbol{n}$ the vector of the N normal modes of the system containing the number of quanta for each mode and χ_0 the zero-point contribution (in cm^{-1}), given by,[45,58]

$$\begin{aligned} 64\chi_0 = &\sum_i k_{iiii} + \frac{7}{9}\sum_i \frac{{k_{iii}}^2}{\omega_i} + 3\sum_i \sum_{j\neq i} \frac{\omega_i {k_{ijj}}^2}{4{\omega_j}^2 - {\omega_i}^2} - 16 \sum_{i<j<k} \frac{\omega_i\omega_j\omega_k {k_{ijk}}^2}{\Delta_{ijk}} \\ &- 16\sum_\tau B_\tau^{\mathrm{eq}} \left[1 + 2\sum_{i<j} \{\zeta_{ij,\tau}\}^2\right] \end{aligned} \tag{5}$$

B_τ^{eq} is a Cartesian element of the inverse inertia tensor at the reference geometry (in cm^{-1}) and $\zeta_{ij,\tau}$ is a Cartesian component of the Coriolis couplings between modes i and j, and Δ_{ijk} is defined as,

$$\Delta_{ijk} = {\omega_i}^4 + {\omega_j}^4 + {\omega_k}^4 - 2\big({\omega_i}^2{\omega_j}^2 + {\omega_i}^2{\omega_k}^2 + {\omega_j}^2{\omega_k}^2\big)$$

k_{ijk} and k_{ijkl} are respectively the third and fourth derivatives of the potential energy V (in cm^{-1}) with respect to the dimensionless normal coordinates $\boldsymbol{q}$, also called cubic and quartic force constants,

$$k_{ijk} = \frac{\partial^3 V}{\partial q_i \partial q_j \partial q_k} \qquad \text{and} \qquad k_{ijkl} = \frac{\partial^4 V}{\partial q_i \partial q_j \partial q_k \partial q_l}$$

$\boldsymbol{\chi}$ is the matrix containing the anharmonic contributions (in cm^{-1}), whose elements are

defined as,

$$16\chi_{ii} = k_{iiii} - \frac{5{k_{iii}}^2}{3\omega_i} - \sum_{j\neq i} \frac{\left(8{\omega_i}^2 - 3{\omega_j}^2\right){k_{iij}}^2}{\omega_j\left(4{\omega_i}^2 - {\omega_j}^2\right)} \tag{6}$$

$$\begin{aligned} 4\chi_{ij} = k_{iijj} &- \frac{2\omega_i {k_{iij}}^2}{\left(4{\omega_i}^2 - {\omega_j}^2\right)} - \frac{2\omega_j {k_{ijj}}^2}{\left(4{\omega_j}^2 - {\omega_i}^2\right)} - \frac{k_{iii}k_{ijj}}{\omega_i} - \frac{k_{jjj}k_{iij}}{\omega_j} \\ &+ \sum_{k\neq i,j}\left[\frac{2\omega_k\left({\omega_i}^2 + {\omega_j}^2 - {\omega_k}^2\right){k_{ijk}}^2}{\Delta_{ijk}} - \frac{k_{iik}k_{jjk}}{\omega_k}\right] + \frac{4\left({\omega_i}^2 + {\omega_j}^2\right)}{\omega_i\omega_j}\sum_{\tau} B_{\tau}^{\mathrm{eq}}\{\zeta_{ij,\tau}\}^2 \end{aligned} \tag{7}$$

All energy derivatives and the Coriolis couplings are expressed in cm^{-1}.

By replacing $\boldsymbol{n}$ in equation 4 with the states of interest, it is straightforward to derive the associated transition energies from the vibrational ground state as $\nu_{\boldsymbol{n}} = \varepsilon_{\boldsymbol{n}} - \varepsilon_{\boldsymbol{0}}$. For the possible states with up to 3 quanta, the corresponding energies are,

Fundamental bands

$$|\,1_i\,\rangle \quad \rightarrow \quad \nu_{1_i} = \omega_i + 2\chi_{ii} + \frac{1}{2}\sum_{j\neq i}\chi_{ij}$$

Overtones

$$|\,2_i\,\rangle \quad \rightarrow \quad \nu_{2_i} = 2\omega_i + 6\chi_{ii} + \sum_{j\neq i}\chi_{ij} = 2\nu_{1_i} + 2\chi_{ii}$$

$$|\,3_i\,\rangle \quad \rightarrow \quad \nu_{3_i} = 3\omega_i + 12\chi_{ii} + \frac{3}{2}\sum_{j\neq i}\chi_{ij} = 3\nu_{1_i} + 6\chi_{ii}$$

Combination bands

$$|\,1_i1_j\,\rangle \quad \rightarrow \quad \nu_{1_i1_j} = \omega_i + \omega_j + 2(\chi_{ii} + \chi_{jj} + \chi_{ij}) + \frac{1}{2}\sum_{k\neq i,j}\{\chi_{ik} + \chi_{jk}\} = \nu_{1_i} + \nu_{1_j} + \chi_{ij}$$

$$|\,2_i1_j\,\rangle \quad \rightarrow \quad \nu_{2_i1_j} = 2\omega_i + \omega_j + 6\chi_{ii} + 2\chi_{jj} + \frac{7}{2}\chi_{ij} + \frac{1}{2}\sum_{k\neq i,j}\{2\chi_{ik} + \chi_{jk}\} = \nu_{2_i} + \nu_{1_j} + 2\chi_{ij}$$

$$\begin{aligned} |\,1_i1_j1_k\,\rangle \quad \rightarrow \quad \nu_{1_i1_j1_k} &= \omega_i + \omega_j + \omega_k + 2(\chi_{ii} + \chi_{jj} + \chi_{kk} + \chi_{ij} + \chi_{ik} + \chi_{jk}) + \frac{1}{2}\sum_{l\neq i,j,k}\{\chi_{il} + \chi_{jl} + \chi_{kl}\} \\ &= \nu_{1_i} + \nu_{1_j} + \nu_{1_k} + \chi_{ij} + \chi_{ik} + \chi_{jk} \end{aligned}$$

Thanks to the availability of simple and general formulas to compute VPT2 energies, their implementation is greatly facilitated and such a feature is now available in various computational chemistry programs. However, a rapid analysis of equations 6 and 7 is enough to highlight one of the major pitfalls in the calculation of VPT2 energies, which is the possible presence of resonance situations where one or more terms in the right-hand side of those equations can be nearly vanishing. Such singularities, called Fermi resonances, of type I ($\omega_i \approx 2\omega_j$) and II ($\omega_i \approx \omega_j + \omega_k$), result in an incorrect account of the anharmonic contributions, with potentially large errors in the computed vibrational energies. Since the probability and the number of occurrences of resonances grow with the number of normal modes, hence the system size, a proper handling of Fermi resonances is required and has been the subject of various studies.[44,45,63–66] Due to the potential impact of this phenomenon on the band positions, a few words will be spent on the possible treatments of resonances. The first step is the identification of the resonant terms, generally done by mean of thresholds on the frequency difference, which can be complemented by additional criteria. An example of the latter is based on the test proposed by Martin and coworkers to evaluate the deviation between the VPT2 result and a model variational calculation by calculating the fourth-order term of an *ad hoc* Taylor expansion series.[63] In this case, the identification of resonant terms will rely on two consecutive tests, first on the magnitude of the frequency difference and then on the Martin test. In the deperturbed VPT2 (DVPT2) approach, terms flagged as resonant are simply ignored in the calculation of $\boldsymbol{\chi}$. To be thorough, the tests are not done on the terms in equations 6 and 7 but on those obtained once every elements in the right-hand side of these equations have been expanded in partial fractions. A drawback of the DVPT2 method is that it corresponds to a truncated VPT2 treatment, with actual contributions of unknown magnitude simply discarded. As the number of resonances, and so of ignored terms, increases, the reliability of the DVPT2 treatment drops. In order to compensate this shortcoming, the discarded terms can be reintroduced in a successive step by using a reduced-dimensionality variational treatment.[45,66] This approach is referred to as the generalized VPT2 (GVPT2)

and can be considered as the method of reference when accuracy is required, thus it has been used in the present work. An alternative approach, initially proposed by Kuhler, Truhlar and Isaacson[64] and named degeneracy-corrected PT2 (DCPT2), relies on a different strategy and is devoid of any threshold. The underlying idea is to replace all potentially resonant terms by a non-resonant form, based on a model variational interaction matrix. A major drawback of this method is the inaccuracy it introduces far from resonance, which can be partially lifted by introducing a transition function to mix the results from the VPT2 and DCPT2 approaches, as done with the hybrid DPCT2-VPT2 (HDCPT2) scheme.[65] While slightly less accurate than GVPT2, HDCPT2 is interesting as a preliminary method to check the reliability of the criteria used to identify the resonant terms, in particular in benchmark studies. Further technical details and tests on those models can be found in Ref.[65]

Transition intensities

The quantities of interest here for IR and VCD are respectively D_{IF} and R_{IF}, given by,

$$D_{IF} = |\langle\, \boldsymbol{\mu} \,\rangle_{I,F}|^2 \tag{8}$$

$$R_{IF} = \Im\left(\langle\, \boldsymbol{\mu} \,\rangle_{I,F} \langle\, \boldsymbol{m} \,\rangle_{F,I}\right) \tag{9}$$

where $\langle\, \boldsymbol{\mu} \,\rangle_{I,F}$ and $\langle\, \boldsymbol{m} \,\rangle_{F,I}$ represents the transition integral of the electric and magnetic dipoles between the initial and final vibrational states, respectively expressed in debye and statA·cm.

The definition of the Raman activity depends on the experimental setup. The most common definition is obtained by assuming that the scattered light is unpolarized and perpendicular to the incident one, which has a perpendicular polarization. In such conditions, S_{IF} is defined as,

$$S_{IF} = 45{a_{I,F}}^2 + 7{g_{I,F}}^2 \tag{10}$$

where the isotropic invariants a and g are respectively the mean isotropic polarizability and

the symmetric anisotropy, given by,

$$
\begin{aligned}
a_{I,F} =& \frac{1}{3}\left[\langle\, \alpha_{xx} \,\rangle_{I,F} + \langle\, \alpha_{yy} \,\rangle_{I,F} + \langle\, \alpha_{zz} \,\rangle_{I,F}\right] \\
g_{I,F} =& \frac{1}{2}\left[\langle\, \alpha_{xx} \,\rangle_{I,F} - \langle\, \alpha_{yy} \,\rangle_{I,F}\right]^2 + \frac{1}{2}\left[\langle\, \alpha_{yy} \,\rangle_{I,F} - \langle\, \alpha_{zz} \,\rangle_{I,F}\right]^2 + \frac{1}{2}\left[\langle\, \alpha_{zz} \,\rangle_{I,F} - \langle\, \alpha_{xx} \,\rangle_{I,F}\right]^2 \\
& + 3\left[\langle\, \alpha_{xy} \,\rangle_{I,F}{}^2 + \langle\, \alpha_{yz} \,\rangle_{I,F}{}^2 + \langle\, \alpha_{zx} \,\rangle_{I,F}{}^2\right]
\end{aligned}
$$

Note that $\boldsymbol{\alpha}$ can be either the static or frequency-dependent polarizability tensor, the derivation presented being independent of the definition of $\boldsymbol{\alpha}$. The Raman activity is often expressed in $\mathring{A}^4$/amu since the first derivatives of the polarizability, which are the only contributing terms at the harmonic level, are often expressed with respect to the mass-weighted normal coordinates. In the present case, the derivatives are expressed with respect to the dimensionless normal coordinates, so S is expressed in $\mathring{A}^6$.

Following the strategy introduced before,[58] a generic property $\boldsymbol{P}$ will be considered from here on, defined by the following relations,

$$\boldsymbol{P} = \boldsymbol{P}^{(0)} + \boldsymbol{P}^{(1)} + \boldsymbol{P}^{(2)} \tag{11}$$

$$\boldsymbol{P}^{(0)} = \boldsymbol{P}^{\mathrm{eq}} + s_0 \sum_{i=1}^{N} \boldsymbol{P}_i (a_i^\dagger + \mathrm{S} a_i) \tag{12}$$

$$\boldsymbol{P}^{(1)} = s_1 \sum_{i=1}^{N}\sum_{j=1}^{N} \boldsymbol{P}_{ji} q_j (a_i^\dagger + \mathrm{S} a_i) \tag{13}$$

$$\boldsymbol{P}^{(2)} = s_2 \sum_{i=1}^{N}\sum_{j=1}^{N}\sum_{k=1}^{N} \boldsymbol{P}_{jki} q_j q_k (a_i^\dagger + \mathrm{S} a_i) \tag{14}$$

where $a_i^\dagger$ and a_i are respectively the creation and annihilation operators. s_0, s_1 and s_2 are constant factors and S represents a sign, so it can be either +1 or -1.

The above expressions can be related to $\boldsymbol{\mu}$, $\boldsymbol{m}$ and $\boldsymbol{\alpha}$ by applying the equivalence relations given in table 1.

Contrary to energies, there is no unique formula to be applied to obtain the transition intensity to any state of interest, but *ad hoc* equations need to be developed for each case.

Table 1: Equivalence relations between the model property $\boldsymbol{P}$ and actual properties $\boldsymbol{\mu}$, $\boldsymbol{m}$ and $\boldsymbol{\alpha}$. $\boldsymbol{A}$ is the atomic axial tensor (AAT).[67]

$\boldsymbol{P}$	$\boldsymbol{P}_0$	$\boldsymbol{P}_i$	$\boldsymbol{P}_{ji}$	$\boldsymbol{P}_{jki}$	s_0	s_1	s_2	S
$\boldsymbol{\mu}$	$\boldsymbol{\mu}^{\text{eq}}$	$\frac{\partial \boldsymbol{\mu}}{\partial q_i}$	$\frac{\partial^2 \boldsymbol{\mu}}{\partial q_i q_j}$	$\frac{\partial^3 \boldsymbol{\mu}}{\partial q_i q_j q_k}$	$\frac{1}{\sqrt{2}}$	$\frac{1}{2\sqrt{2}}$	$\frac{1}{6\sqrt{2}}$	$+1$
$\boldsymbol{m}$	$\boldsymbol{0}$	$\boldsymbol{A}_i$	$\frac{\partial \boldsymbol{A}_i}{\partial q_j}$	$\frac{\partial^2 \boldsymbol{A}_i}{\partial q_j q_k}$	$\frac{\imath\hbar}{\sqrt{2}}$	$\frac{\imath\hbar}{\sqrt{2}}$	$\frac{\imath\hbar}{2\sqrt{2}}$	-1
$\boldsymbol{\alpha}$	$\boldsymbol{\alpha}^{\text{eq}}$	$\frac{\partial \boldsymbol{\alpha}}{\partial q_i}$	$\frac{\partial^2 \boldsymbol{\alpha}}{\partial q_i q_j}$	$\frac{\partial^3 \boldsymbol{\alpha}}{\partial q_i q_j q_k}$	$\frac{1}{\sqrt{2}}$	$\frac{1}{2\sqrt{2}}$	$\frac{1}{6\sqrt{2}}$	$+1$

The machinery used in this work is based on the Rayleigh-Schrödinger perturbation theory and has been detailed in Ref.[58] The present discussion will focus on the main steps of the procedure used to derive the transition integrals at the VPT2 level. The starting point is the transition integral $\langle\, \boldsymbol{P} \,\rangle_{I,F}$,

$$\langle\, \boldsymbol{P} \,\rangle_{I,F} = \frac{\langle\, \psi_I^v \mid \boldsymbol{P}^{\text{e}} \mid \psi_F^v \,\rangle}{\sqrt{\langle\, \psi_I^v \mid \psi_I^v \,\rangle \langle\, \psi_F^v \mid \psi_F^v \,\rangle}} \tag{15}$$

where ψ^v represents the vibrational wavefunction, and $\boldsymbol{P}^{\text{e}}$ is the expected value of $\boldsymbol{P}$ obtained from electronic structure calculations ($\boldsymbol{P}^{\text{e}} = \langle\, \phi_I \mid \boldsymbol{P} \mid \phi_I \,\rangle$. In the following, the superscript "e" will be dropped.

Equation 15 is then developed by expanding the vibrational wavefunction and the property up to the second perturbative order. The various terms are then collected by overall order and only those up to the second order are kept. It should be noted that the denominator, which corresponds to the normalization condition, is also simplified by applying a Taylor expansion up to the second order. The different terms of interest are,

$$\langle \boldsymbol{P} \rangle_{I,F} = \langle \boldsymbol{P} \rangle_{I,F}{}^{(0)} + \langle \boldsymbol{P} \rangle_{I,F}{}^{(1)} + \langle \boldsymbol{P} \rangle_{I,F}{}^{(2)} \tag{16}$$

$$\langle \boldsymbol{P} \rangle_{I,F}{}^{(0)} = \langle \psi_I^{v(0)} \mid \boldsymbol{P}^{(0)} \mid \psi_F^{v(0)} \rangle \tag{17}$$

$$\langle \boldsymbol{P} \rangle_{I,F}{}^{(1)} = \langle \psi_I^{v(0)} \mid \boldsymbol{P}^{(1)} \mid \psi_F^{v(0)} \rangle + \langle \psi_I^{v(1)} \mid \boldsymbol{P}^{(0)} \mid \psi_F^{v(0)} \rangle + \langle \psi_I^{v(0)} \mid \boldsymbol{P}^{(0)} \mid \psi_F^{v(1)} \rangle \tag{18}$$

$$\begin{aligned} \langle \boldsymbol{P} \rangle_{I,F}{}^{(2)} = & \langle \psi_I^{v(0)} \mid \boldsymbol{P}^{(2)} \mid \psi_F^{v(0)} \rangle + \langle \psi_I^{v(2)} \mid \boldsymbol{P}^{(0)} \mid \psi_F^{v(0)} \rangle + \langle \psi_I^{v(0)} \mid \boldsymbol{P}^{(0)} \mid \psi_F^{v(2)} \rangle \\ & + \langle \psi_I^{v(1)} \mid \boldsymbol{P}^{(1)} \mid \psi_F^{v(0)} \rangle + \langle \psi_I^{v(0)} \mid \boldsymbol{P}^{(1)} \mid \psi_F^{v(1)} \rangle + \langle \psi_I^{v(1)} \mid \boldsymbol{P}^{(0)} \mid \psi_F^{v(1)} \rangle \\ & - \frac{\langle \psi_I^{v(0)} \mid \boldsymbol{P}^{(0)} \mid \psi_F^{v(0)} \rangle}{2} \left[\langle \psi_F^{v(1)} \mid \psi_F^{v(1)} \rangle + \langle \psi_I^{v(1)} \mid \psi_I^{v(1)} \rangle \right] \end{aligned} \tag{19}$$

As a reminder, the first- and second-order perturbative wavefunctions are given by,

$$| \psi_r^{v(1)} \rangle = \sum_{s \neq r} \frac{\langle \psi_s^{v(0)} \mid \hat{H}^{(1)} \mid \psi_r^{v(0)} \rangle}{\varepsilon_r{}^{(0)} - \varepsilon_s{}^{(0)}} | \psi_s^{v(0)} \rangle \tag{20}$$

$$\begin{aligned} | \psi_r^{v(2)} \rangle = & \sum_{s \neq r} \sum_{t \neq r} \frac{\langle \psi_s^{v(0)} \mid \hat{H}^{(1)} \mid \psi_t^{v(0)} \rangle \langle \psi_t^{v(0)} \mid \hat{H}^{(1)} \mid \psi_r^{v(0)} \rangle}{\left(\varepsilon_r{}^{(0)} - \varepsilon_t{}^{(0)}\right)\left(\varepsilon_r{}^{(0)} - \varepsilon_s{}^{(0)}\right)} | \psi_s^{v(0)} \rangle \\ & + \sum_{s} \frac{\langle \psi_s^{v(0)} \mid \hat{H}^{(2)} \mid \psi_r^{v(0)} \rangle}{\varepsilon_r{}^{(0)} - \varepsilon_s{}^{(0)}} | \psi_s^{v(0)} \rangle \end{aligned} \tag{21}$$

with $\hat{H}^{(1)}$ and $\hat{H}^{(2)}$ the first and second perturbation orders of the Watson Hamiltonian.[32]

The terms in equations 17 to 19 are then developed for the transitions of interest and the non-null elements are collected in a single equation. In order to assist the derivation and ensure that all terms have been properly accounted for, an *ad hoc* program had been initially written and further refined to support transition integrals to 3-quanta states.

For fundamental bands, the resulting equation is reported below,[58]

$$
\begin{aligned}
\langle \boldsymbol{P} \rangle_{0,1_i} = {} & s_0 \times \mathrm{S} \times \boldsymbol{P}_i + \frac{s_2}{2} \sum_j \{\boldsymbol{P}_{jij} + \boldsymbol{P}_{ijj} + \mathrm{S}\boldsymbol{P}_{jji}\} - \frac{s_0}{8} \sum_{jk} k_{ijkk} \boldsymbol{P}_j \left[\frac{1}{\omega_i + \omega_j} - \frac{\mathrm{S}(1-\delta_{ij})}{\omega_i - \omega_j} \right] \\
& - \frac{s_1}{8} \sum_{jk} \left\{ k_{ijk} \left(\boldsymbol{P}_{jk} + \boldsymbol{P}_{kj} \right) \left(\frac{1}{\omega_i + \omega_j + \omega_k} - \frac{\mathrm{S}}{\omega_i - \omega_j - \omega_k} \right) + \frac{k_{jkk}}{\omega_j} \left[2\mathrm{S}\boldsymbol{P}_{ji} + (1+\mathrm{S})\boldsymbol{P}_{ij} \right] \right\} \\
& + \frac{s_0}{2} \sum_{jk} \left(\sum_\tau B_\tau^{\mathrm{eq}} \zeta_{ik,\tau} \zeta_{jk,\tau} \right) \boldsymbol{P}_j \left\{ \frac{\sqrt{\omega_i \omega_j}}{\omega_k} \left(\frac{1}{\omega_i + \omega_j} + \frac{\mathrm{S}(1-\delta_{ij})}{\omega_i - \omega_j} \right) - \frac{\omega_k}{\sqrt{\omega_i \omega_j}} \left(\frac{1}{\omega_i + \omega_j} - \frac{\mathrm{S}(1-\delta_{ij})}{\omega_i - \omega_j} \right) \right\} \\
& + \frac{s_0}{16} \sum_{jkl} k_{ikl} k_{jkl} \boldsymbol{P}_j \Bigg\{ (1-\delta_{ij})(1-\delta_{ik})(1-\delta_{il}) \Bigg[\frac{1}{(\omega_i + \omega_j)(\omega_j + \omega_k + \omega_l)} - \frac{\mathrm{S}}{(\omega_i - \omega_j)(\omega_j + \omega_k + \omega_l)} \\
& \quad + \frac{\mathrm{S}}{(\omega_i + \omega_k + \omega_l)(\omega_j + \omega_k + \omega_l)} - \frac{1}{(\omega_i - \omega_k - \omega_l)(\omega_j + \omega_k + \omega_l)} + \frac{\mathrm{S}}{(\omega_i - \omega_j)(\omega_i - \omega_k - \omega_l)} \\
& \quad + \frac{1}{(\omega_i + \omega_j)(\omega_i + \omega_k + \omega_l)} \Bigg] \\
& \quad + \delta_{ij}(1+\delta_{ik})(1-\delta_{il}) \Bigg[\frac{1}{2\omega_i(\omega_i + \omega_k + \omega_l)} - \frac{1}{2\omega_i(\omega_i - \omega_k - \omega_l)} + \frac{\mathrm{S}}{2(\omega_i + \omega_k + \omega_l)^2} \\
& \quad - \frac{\mathrm{S}}{2(\omega_i - \omega_k - \omega_l)^2} \Bigg] \\
& \quad + (1-\delta_{ij})(1-\delta_{ik})\delta_{il} \Bigg[\frac{1}{\omega_k(\omega_i + \omega_j)} + \frac{2}{(2\omega_i + \omega_k)(\omega_i + \omega_j)} + \frac{3}{(\omega_i + \omega_j)(\omega_i + \omega_j + \omega_k)} \\
& \quad + \frac{\mathrm{S}}{(\omega_i - \omega_j)(\omega_i - \omega_j - \omega_k)} - \frac{2\mathrm{S}}{(\omega_i - \omega_j)(\omega_i + \omega_j + \omega_k)} - \frac{3\mathrm{S}}{\omega_k(\omega_i - \omega_j)} \\
& \quad - \frac{\mathrm{S}}{\omega_k(\omega_i - \omega_j - \omega_k)} + \frac{2\mathrm{S}}{(2\omega_i + \omega_k)(\omega_i + \omega_j + \omega_k)} + \frac{3}{\omega_k(\omega_i + \omega_j + \omega_k)} \Bigg] \Bigg\} \\
& + k_{ijk} k_{llk} \boldsymbol{P}_j \Bigg\{ \frac{\delta_{ij}}{\omega_i \omega_k} \left(1 + \frac{\delta_{ik}\delta_{il}(6-4\mathrm{S})}{9} \right) \\
& \quad + (1-\delta_{ij})(1-\delta_{ik})(1-\delta_{il}) \Bigg[\frac{1}{(\omega_i + \omega_j)(\omega_i + \omega_j + \omega_k)} + \frac{1}{\omega_k(\omega_i + \omega_j)} - \frac{\mathrm{S}}{\omega_k(\omega_i - \omega_j)} \\
& \quad + \frac{\mathrm{S}}{(\omega_i - \omega_j)(\omega_i - \omega_j - \omega_k)} + \frac{1}{\omega_k(\omega_i + \omega_j + \omega_k)} - \frac{\mathrm{S}}{\omega_k(\omega_i - \omega_j - \omega_k)} \Bigg] \\
& \quad + \delta_{ik}(1-\delta_{ij}) \Bigg[(1+\delta_{il}) \left(\frac{1}{(2\omega_i + \omega_j)(\omega_i + \omega_j)} - \frac{\mathrm{S}}{\omega_i(\omega_i - \omega_j)} + \frac{1}{\omega_i(2\omega_i + \omega_j)} \right) \\
& \quad + \delta_{il} \left(\frac{1}{3\omega_i(\omega_i + \omega_j)} + \frac{\mathrm{S}}{3\omega_i(2\omega_i + \omega_j)} - \frac{\mathrm{S}}{(\omega_i - \omega_j)(2\omega_i + \omega_j)} \right) \\
& \quad + \frac{1}{\omega_i(\omega_i + \omega_j)} - \frac{\mathrm{S}}{\omega_j(\omega_i - \omega_j)} + \frac{\mathrm{S}}{\omega_i \omega_j} \Bigg] \Bigg\}
\end{aligned}
\tag{22}
$$

where δ_{ij} is the Kronecker delta. From an analysis of table 1, and more precisely the case of the magnetic dipole with the axial atomic tensor, it should be noted the indices of $\boldsymbol{P}_{ij}$ and $\boldsymbol{P}_{ijk}$ may not be freely interchangeable. For this reason, equation 22 and the following equations are written with the most general case in mind.

For overtones ($\langle\, \boldsymbol{P} \,\rangle_{0,2_i}$) and combination bands ($\langle\, \boldsymbol{P} \,\rangle_{0,1_i1_j}$) of two quanta, a common formula can be used to compute the transition integral,

$$\begin{aligned} \langle\, \boldsymbol{P} \,\rangle_{0,(1+\delta_{ij})_i(1-\delta_{ij})_j} =& \sqrt{\frac{2}{1+\delta_{ij}}} \times \left[\frac{s_1 \times \mathrm{S}}{2} \left(\boldsymbol{P}_{ij} + \boldsymbol{P}_{ji}\right) \right. \\ & \left. + \frac{s_0}{4} \sum_k k_{ijk} \boldsymbol{P}_k \left(\frac{\mathrm{S}}{\omega_i + \omega_j - \omega_k} - \frac{1}{\omega_i + \omega_j + \omega_k} \right) \right] \end{aligned} \tag{23}$$

Note that in the original paper,[58] the second term was incorrectly reported, with "$k_{ijk}\boldsymbol{P}_k$" missing.

In the same way, a common formula can be derived for the transition integrals to overtones

($\langle \boldsymbol{P} \rangle_{0,3_i}$) and combinations bands ($\langle \boldsymbol{P} \rangle_{0,2_i1_j}$ and $\langle \boldsymbol{P} \rangle_{0,1_i1_j1_k}$) of 3 quanta,

$$
\begin{aligned}
&\langle \boldsymbol{P} \rangle_{0,(1+\delta_{ij}+\delta_{ik})_i(1-\delta_{ij})_j(1-\delta_{ik})_k} = \\
&\quad A \times s_2 \times S\left(\boldsymbol{P}_{jki} + \boldsymbol{P}_{ikj} + \boldsymbol{P}_{ijk}\right) \\
&\quad + A\frac{s_0}{4}\sum_l k_{ijkl}\boldsymbol{P}_l\left[\frac{\mathrm{S}}{\omega_i+\omega_j+\omega_k-\omega_l} - \frac{1}{\omega_i+\omega_j+\omega_k+\omega_l}\right] \\
&\quad + A\frac{s_0}{2}\sum_\tau\sum_l B_\tau^{\mathrm{eq}}\boldsymbol{P}_l\left[\zeta_{ij,\tau}\zeta_{kl,\tau}\left(\frac{\omega_i\omega_k}{\omega_j\omega_l}+\frac{\omega_j\omega_l}{\omega_i\omega_k}+\frac{\omega_i\omega_l}{\omega_j\omega_k}+\frac{\omega_j\omega_k}{\omega_i\omega_l}\right) + \zeta_{ik}^\tau\zeta_{jl}^\tau\left(\frac{\omega_i\omega_j}{\omega_k\omega_l}+\frac{\omega_k\omega_l}{\omega_i\omega_j}+\frac{\omega_i\omega_l}{\omega_j\omega_k}+\frac{\omega_j\omega_k}{\omega_i\omega_l}\right)\right. \\
&\qquad \left. + \zeta_{il}^\tau\zeta_{jk}^\tau\left(\frac{\omega_i\omega_j}{\omega_k\omega_l}+\frac{\omega_k\omega_l}{\omega_i\omega_j}+\frac{\omega_i\omega_k}{\omega_j\omega_l}+\frac{\omega_j\omega_l}{\omega_i\omega_k}\right)\right] \times \left[\frac{1}{\omega_i+\omega_j+\omega_k+\omega_l} - \frac{\mathrm{S}}{\omega_i+\omega_j+\omega_k-\omega_l}\right] \\
&\quad + A\frac{s_1}{4}\sum_l\left\{k_{ijl}\left[\frac{\mathrm{S}\times(\boldsymbol{P}_{kl}+\boldsymbol{P}_{lk})}{\omega_i+\omega_j-\omega_l} - \frac{\boldsymbol{P}_{kl}+\mathrm{S}\times\boldsymbol{P}_{lk}}{\omega_i+\omega_j+\omega_l}\right] + k_{ikl}\left[\frac{\mathrm{S}\times(\boldsymbol{P}_{jl}+\boldsymbol{P}_{lj})}{\omega_i+\omega_k-\omega_l} - \frac{\boldsymbol{P}_{jl}+\mathrm{S}\times\boldsymbol{P}_{lj}}{\omega_i+\omega_k+\omega_l}\right]\right. \\
&\qquad \left. + k_{jkl}\left[\frac{\mathrm{S}\times(\boldsymbol{P}_{il}+\boldsymbol{P}_{li})}{\omega_j+\omega_k-\omega_l} - \frac{\boldsymbol{P}_{il}+\mathrm{S}\times\boldsymbol{P}_{li}}{\omega_j+\omega_k+\omega_l}\right]\right\} \\
&\quad + A\frac{s_0}{8}\sum_{l,m}k_{ijl}k_{klm}\boldsymbol{P}_m\left[\frac{1}{(\omega_l+\omega_j+\omega_i)(\omega_m+\omega_k+\omega_j+\omega_i)} + \frac{1}{(\omega_l-\omega_j-\omega_i)(\omega_m+\omega_k+\omega_j+\omega_i)}\right. \\
&\qquad \left. + \frac{\mathrm{S}}{(\omega_l+\omega_j+\omega_i)(\omega_m-\omega_k-\omega_j-\omega_i)} + \frac{\mathrm{S}}{(\omega_l-\omega_j-\omega_i)(\omega_m-\omega_k-\omega_j-\omega_i)}\right] \\
&\quad + k_{ikl}k_{jlm}\boldsymbol{P}_m\left[\frac{1}{(\omega_l+\omega_k+\omega_i)(\omega_m+\omega_k+\omega_j+\omega_i)} + \frac{1}{(\omega_l-\omega_k-\omega_i)(\omega_m+\omega_k+\omega_j+\omega_i)}\right. \\
&\qquad \left. + \frac{\mathrm{S}}{(\omega_l+\omega_k+\omega_i)(\omega_m-\omega_k-\omega_j-\omega_i)} + \frac{\mathrm{S}}{(\omega_l-\omega_k-\omega_i)(\omega_m-\omega_k-\omega_j-\omega_i)}\right] \\
&\quad + k_{jkl}k_{ilm}\boldsymbol{P}_m\left[\frac{1}{(\omega_l+\omega_k+\omega_j)(\omega_m+\omega_k+\omega_j+\omega_i)} + \frac{1}{(\omega_l-\omega_k-\omega_j)(\omega_m+\omega_k+\omega_j+\omega_i)}\right. \\
&\qquad \left. + \frac{\mathrm{S}}{(\omega_l+\omega_k+\omega_j)(\omega_m-\omega_k-\omega_j-\omega_i)} + \frac{\mathrm{S}}{(\omega_l-\omega_k-\omega_j)(\omega_m-\omega_k-\omega_j-\omega_i)}\right]
\end{aligned}
\tag{24}
$$

with

$$A = \frac{\sqrt{(1+\delta_{ij}+\delta_{ik})!}}{(1+\delta_{ij}+\delta_{ik})!}$$

.

It should be noted that, while the definition of a unique formula like equation 24 is convenient from a theoretical point of view, a direct implementation may suffer from low

performance since several terms can be combined or ignored for the overtone and the "2_i1_j" cases. More compact formulas for these two cases are provided in appendix.

To be complete, for transitions to states with 4 quanta only two terms of opposite signs remain at the VPT2 level. As a result, the intensity is systematically null. Consequently, transitions to states with 4 quanta will require a higher level of perturbation theory (VPT4 for instance) or a more accurate variational approach.

An important final point of this discussion regards the specific problem of the magnetic dipole. Indeed, the electronic transition magnetic dipole moment within the Born-Oppenheimer (BO) approximation, gives vanishing contributions for vibrational transitions from the ground state. In order to overcome this issue, contributions from excited electronic states[68] are included by applying a first-order perturbative correction to the BO approximation. Within the simple perturbation theory (SPT), additional terms arise due to the non-commuting character of the nuclear kinetic operator and the electronic wavefunction,[69]

$$\langle \boldsymbol{m} \rangle_{I,F} = \frac{\langle \psi_I^v \mid \boldsymbol{m}^{\mathrm{e}} \mid \psi_F^v \rangle}{\sqrt{\langle \psi_I^v \mid \psi_I^v \rangle \langle \psi_F^v \mid \psi_F^v \rangle}} - \frac{\langle \psi_F^v \mid \boldsymbol{m}^{\mathrm{e}} \mid \psi_I^v \rangle}{\sqrt{\langle \psi_I^v \mid \psi_I^v \rangle \langle \psi_F^v \mid \psi_F^v \rangle}} \tag{25}$$

To obtain the correct transition integral for the magnetic dipole, it is necessary to account for the second term in equation 25 . The corresponding formulas are very similar to equations 22, 23 and 24, thus it is convenient to define them with respect to the latter,

$$\langle \boldsymbol{P} \rangle_{1_i,0} = \mathrm{S} \times \langle \boldsymbol{P} \rangle_{0,1_i} + \frac{s_2}{2}(1-\mathrm{S}) \sum_j (\boldsymbol{P}_{ijj} + \boldsymbol{P}_{jij}) \tag{26}$$

$$\langle \boldsymbol{P} \rangle_{(1+\delta_{ij})_i(1-\delta_{ij})_j,0} = \mathrm{S} \times \langle \boldsymbol{P} \rangle_{0,(1+\delta_{ij})_i(1-\delta_{ij})_j} \tag{27}$$

$$\langle \boldsymbol{P} \rangle_{(1+\delta_{ij}+\delta_{ik})_i(1-\delta_{ij})_j(1-\delta_{ik})_k,0} = \mathrm{S} \times \langle \boldsymbol{P} \rangle_{0,(1+\delta_{ij}+\delta_{ik})_i(1-\delta_{ij})_j(1-\delta_{ik})_k} \tag{28}$$

As a result, the transition moment of the magnetic dipole in equation 9 with the SPT

correction to the BO approximation are,

$$\langle\, \boldsymbol{m} \,\rangle^{\mathrm{SPT}}_{1i,0} = -2\langle\, \boldsymbol{m} \,\rangle^{\mathrm{BO}}_{0,1_i} + s_2 \sum_j (\boldsymbol{P}_{ijj} + \boldsymbol{P}_{jij}) \tag{29}$$

$$\langle\, \boldsymbol{m} \,\rangle^{\mathrm{SPT}}_{(1+\delta_{ij})_i(1-\delta_{ij})_j,0} = -2\langle\, \boldsymbol{m} \,\rangle^{\mathrm{BO}}_{0,(1+\delta_{ij})_i(1-\delta_{ij})_j} \tag{30}$$

$$\langle\, \boldsymbol{m} \,\rangle^{\mathrm{SPT}}_{(1+\delta_{ij}+\delta_{ik})_i(1-\delta_{ij})_j(1-\delta_{ik})_k,0} = -2\langle\, \boldsymbol{m} \,\rangle^{\mathrm{BO}}_{0,(1+\delta_{ij}+\delta_{ik})_i(1-\delta_{ij})_j(1-\delta_{ik})_k} \tag{31}$$

where the superscript "BO" refers to the transition moments computed with the equations 22 to 24.

Similarly to energies, transitions intensities at the VPT2 level suffer from the problem of resonances. An analysis of equations 22 to 24 shows that the presence of Fermi resonances can also lead in this case to incorrect accounts of the anharmonic contributions and result in wrong calculated intensities. However, equations 22 and 24 contain each one an additional potential source of singularities, if $\omega_j \approx \omega_i$ for fundamental bands and if $\omega_l \approx \omega_i + \omega_j + \omega_k$ for 3-quanta transitions. While the case of Fermi resonance also in transition intensities has been already considered in the literature,[44,57] the problem of numerical instability due to 1-1 and 1-3 resonances in the calculation of transition moments and how to handle it has been generally ignored. Following the strategy used before and by other authors,[57] the Fermi resonances will be treated in the same way as for energy, using the same definition of the resonant terms. For 1-1 (eq. 22) and 1-3 (eq. 24) resonances, an *ad hoc* double criterion will be used, based on the magnitude of the frequency difference in the denominator and of the numerator. A comparison of equations 22 and 24 shows that the terms where such resonances can arise are very similar, so the same thresholds can be used for the second criterion (numerator). Regarding the magnitude of the denominator, the most critical case of 1-1 resonances is due to near-degenerate modes (for instance the symmetric and antisymmetric C-H stretchings of methyl groups), so a low value can be used as threshold. For 1-3, a larger value must be used in order to compensate for the numerical inaccuracies. More details on those thresholds will be given in the computational details.

Computational details

Calculations were performed for isolated molecules with DFT, using the B3LYP functional coupled to the SNSD[62] basis set. The latter has been built from the N07D basis set[70–72] by consistently including diffuse s functions on all atoms, and one set of diffuse polarized functions (d on heavy atoms and p on hydrogens). It was devised to provide an optimal ratio between size and reliability to compute frequencies and molecular properties. As a result, it is well suited to treat medium-to-large molecules and was the reason for its choice here. DFT calculations have been done with an ultrafine grid for the numerical integrations (199 radial points, 590 angular points), and default tight density-based convergence criteria for the self-consistent field step. In order to ensure that a proper minimum of the PES is reached, geometry optimization were carried out with very tight convergence criteria (convergence on forces: 10^{-6} Hartree/Bohr, convergence on estimated displacement: $4 \cdot 10^{-6}$ Bohr).

Anharmonic data, were calculated by numerical differentiations, following the scheme described in ref.,[45] using the default setting of 0.01 $\sqrt{\text{amu}} \cdot$ Å along each mass-weighted normal coordinate,

$$k_{ijk} = \frac{1}{3}\left[\sqrt{\frac{\hbar}{2\pi c\omega_i}}\frac{k_{jk}(+\delta Q_i) - k_{jk}(-\delta Q_i)}{2\delta Q_i} + \sqrt{\frac{\hbar}{2\pi c\omega_j}}\frac{k_{ik}(+\delta Q_j) - k_{ik}(-\delta Q_j)}{2\delta Q_j} + \sqrt{\frac{\hbar}{2\pi c\omega_k}}\frac{k_{ij}(+\delta Q_k) - k_{ij}(-\delta Q_k)}{2\delta Q_k}\right] \tag{32}$$

$$k_{iijk} = \frac{\hbar}{2\pi c\omega_i}\frac{k_{jk}(+\delta Q_i) - k_{jk}(-\delta Q_i)}{{\delta Q_i}^2} \tag{33}$$

$$k_{iijj} = \frac{1}{2}\left[\frac{\hbar}{2\pi c\omega_i}\frac{k_{jj}(+\delta Q_i) - k_{jj}(-\delta Q_i)}{{\delta Q_i}^2} + \frac{\hbar}{2\pi c\omega_j}\frac{k_{ii}(+\delta Q_j) - k_{ii}(-\delta Q_j)}{{\delta Q_j}^2}\right] \tag{34}$$

$$\boldsymbol{P}_{ji} = \sqrt{\frac{\hbar}{2\pi c\omega_j}}\frac{\boldsymbol{P}_i(+\delta Q_j) - \boldsymbol{P}_i(-\delta Q_j)}{2\delta Q_j} \tag{35}$$

$$\boldsymbol{P}_{jji} = \frac{\hbar}{2\pi c\omega_j}\frac{\boldsymbol{P}_i(+\delta Q_j) - \boldsymbol{P}_i(-\delta Q_j)}{{\delta Q_j}^2} \tag{36}$$

where k_{ij} is the analytic second derivative of the energy with respect to dimensionless normal

coordinates q_i and q_j. Note that if the indices of $\boldsymbol{P}$ are interchangeable as it is the case with the electric dipole and polarizability tensor, $\boldsymbol{P}_{ji}$ can be obtained in two different ways, and the average is used in this case,

$$\boldsymbol{P}_{ji} = \frac{1}{2}\left[\sqrt{\frac{\hbar}{2\pi c\omega_i}}\frac{\boldsymbol{P}_j(+\delta Q_i) - \boldsymbol{P}_j(-\delta Q_i)}{2\delta Q_i} + \sqrt{\frac{\hbar}{2\pi c\omega_j}}\frac{\boldsymbol{P}_i(+\delta Q_j) - \boldsymbol{P}_i(-\delta Q_j)}{2\delta Q_j}\right] \tag{37}$$

The previous equations are intended for the general case, where the numerical differentiation is carried out over all the normal coordinates. In presence of reduced-dimensionality schemes where a subset of the normal modes are considered active and only the corresponding normal coordinates are used for the displacements, some of the constants may not be computed or only a reduced number of combinations could be available. In the latter case, the missing terms in the previous equations are simply ignored and the leading fraction is corrected according to the number of terms actually used.[62,73]

Based on the data available from the numerical differentiations, some comments on the feasibility of the computation of transitions integrals are in order. For the transition to fundamental bands (equation 22), the off-diagonal elements $\boldsymbol{P}_{ijj}$ and $\boldsymbol{P}_{jij}$ (both corresponding to $\partial^2\boldsymbol{A}_j/\partial q_i\partial q_j$) are not available, which could result in a potential issue in the reliability of the calculations. However, once the SPT correction to the BO approximation is applied, those terms are canceled out so the transition magnetic dipole moment can be calculated without any problem. Equation 23 raises no particular issue. The main problem is with equation 24, that is the transitions to 3-quanta states. $\langle\,\boldsymbol{P}\,\rangle_{0,1_i1_j1_k}$ requires some off-diagonal terms, namely k_{ijkl} and $\boldsymbol{P}_{ijk}$, which are not available if $l \neq k \neq j \neq i$. While such terms are unlikely to give significant contributions, in particular with respect to the other terms, one should remain cautious of the reliability of the results with the missing terms. Another problem arises for $\langle\,\boldsymbol{P}\,\rangle_{0,2_i1_j}$ in the specific case of the magnetic dipole, since the convenient cancellation of the off-diagonal terms $\boldsymbol{P}_{ijj}$ and $\boldsymbol{P}_{jij}$ does not happen here. This problem is not present for IR and Raman, the former being the spectroscopy of interest in the present

case.

Regarding the treatment of resonances, the GVPT2 approach has been used for the energies. For the deperturbed step, the following criteria were used to identify the resonant terms

Type	Frequency test	Martin test
I	$\lvert\omega_i - 2\omega_j\rvert \leq 200$ cm^{-1}	$\Delta^1_{ij} \geq 1$ cm^{-1}
II	$\lvert\omega_i - \omega_j - \omega_k\rvert \leq 200$ cm^{-1}	$\Delta^2_{ijk} \geq 1$ cm^{-1}

where Δ^1_{ij} and Δ^2_{ijk} are the so-called Martin parameters defined in ref.[45] The test is carried out in two successive steps, first on the frequency difference and then on the magnitude (Δ^1_{ij} and Δ^2_{ijk}). This procedure reduces the time needed for the test but also limits the risk of a false positive where a term is incorrectly flagged as resonant based on the sole Martin test.

For intensities, the same tests as for energies have been used to identify Fermi resonances. In practice, the set of resonant terms is built once, during the vibrational energy calculation step and applied to the energies and successively to the transition intensities. Regarding the 1-1 and 1-3 resonances described in the previous section, the test proposed in Ref.[58] has been used and extended here. For 1-1 resonance, the criterion on the frequency difference is, $\Delta^{1\text{-}1}_{\omega} = \lvert\omega_j - \omega_i\rvert \leq 2$ cm^{-1}, while a larger value is used for 1-3 resonances, $\Delta^{1\text{-}3}_{\omega} = \lvert\omega_l - \omega_i - \omega_j - \omega_k\rvert \leq 20$ cm^{-1}. The terms with risks of singularities due to 1-1 and 1-3 resonances derive from the same perturbative term. As a result, the same criteria are used regarding the magnitude of the numerators, which are divided in two categories based on their unit. The Coriolis and quartic terms have numerator in cm^{-1}, while those of the cubic terms are in cm^{-2}, so two distinct tests are defined, respectively $K_1^{1\text{-n}}$ and $K_2^{1\text{-n}}$.

$$\left|K_1^{1\text{-n}}\right| \geq 10 \text{ cm}^{-1} \qquad \text{and} \qquad \left|K_2^{1\text{-n}}\right| \geq 10 \text{ cm}^{-2}$$

The equations presented above have been implemented in a locally modified version of Gaussian.[10]

Results

Due to the strong decrease of intensity observed at higher energy, IR spectra over large energy ranges are often divided in regions, generally correlated to the X–H stretching overtones, in particular the C–H ones. The C–H stretching bands represent interesting markers for the study of IR spectra of organic systems, thanks to their strong intensities and their limited couplings with other modes. The analysis of overtone spectra is then generally based on the local mode approach (see Ref.[74] for a discussion on the underlying theory), where empirical parameters are used to evaluate the anharmonic contributions and interpret the observed spectra. The study of C–H stretchings can be facilitated by choosing well suited molecules, which explains the extensive study of alkenes and alkanes.[74–80] As a result, a large quantity of reference data has been collected and can be used for a preliminary validation of the procedure presented here. It should be noted that for CH stretchings, the energy levels at the VPT2 level are equivalent to those of the Morse potential, so it is expected that the perturbative approach remains accurate also for higher overtones.[81] As previously stated by Stanton and coworkers,[82] this observation cannot be generalized to the case of the property surface, which can have a significantly different form.

Nitric acid The first case study, which will serve for a preliminary validation of the implementation, is the infrared spectrum of nitric acid (depicted in Fig. 1). Due to the interest it presents in the understanding of the depletion process of stratospheric ozone, this molecule has been extensively studied and a large number of highly resolved spectra, including infrared, has been recorded.[83] Moreover, the IR spectrum of HNO_3 has also been simulated at the VPT2 level over a large energy range (0–11000 cm^{-1}) and directly compared to highly resolved experimental measurements by Vaida and coworkers,[84] facilitating the comparison with the data computed here. As a first remark, the protocol used for the calculation of the intensities in ref.[84] differs from the one presented here. Instead of eqs. 22 to 24, the transition moments are obtained as sums over states by explicitly considering all terms in

eq. 11, which makes such treatment rather cumbersome. Anyway, the results are expected to be the same as with the present formulas for the same set of initial data (energy and property derivatives).[51] Fundamental wavenumbers are reported in Table 2 together with the corresponding description of the associated vibrations and experimental frequencies.[83] The overall agreement with experimental values is rather good with the main discrepancies associated to modes 1, 2 and 9. For overtones and combination bands, only those whose energy is reported in Ref.[84] are gathered in Table 3. All calculated data taken from Ref.[84] were obtained at the CCSD(T)[85] level of theory with the atomic natural orbital (ANO)[86] basis set. In order to make the comparison with those values possible, the same protocol was followed. The general principle is to associate the discrepancies between the experimental and computed energies to the harmonic part and systematically correct each transition energy with an *ad hoc* contribution. To do so, the shift associated to each mode is obtained for each fundamental band as, $\Delta_i = \nu_i^{\text{exp}} - \nu_{1_i}$. Then, the energy for each overtone and combination state is calculated as,

$$\varepsilon_{\boldsymbol{n}} = \chi_0 + \sum_i^N (\omega_i + \Delta_i)\left(n_i + \frac{1}{2}\right) + \sum_i^N \sum_{j=i}^N \chi_{ij}\left(n_i + \frac{1}{2}\right)\left(n_j + \frac{1}{2}\right)$$

the non-corrected (ν) and corrected (ν^{corr}) results are given in Table 3.

The method is similar to the hybrid scheme used by various authors[87–96] to reach an optimal balance between accuracy and computational cost, with a higher level of theory employed for the harmonic part and a more affordable one for the anharmonic part. The basic difference is that here, only one level of theory is employed and the harmonic part is corrected to fit a set of reference data. In practice, this also has an impact on the conversion of anharmonic data to get derivatives with respect to dimensionless normal coordinates. Indeed, the numerical differentiations are done along mass-weighted normal coordinates. This means that the higher level of theory in the "*ab initio*" hybrid scheme can also be used in the conversion process to further improve the quality of the calculations, which is not

possible in the "fitting" approach, except by mean of an iterative procedure to converge to the reference data.

Considering first the experimental results, the average error is rather small with the main discrepancies associated to states where the H–ON bending mode (mode 4) is involved ($|\,2_4\,\rangle$, $|\,3_4\,\rangle$, $|\,1_4 1_1\,\rangle$ and $|\,2_4 1_1\,\rangle$ and $|\,1_4 2_1\,\rangle$), which hints at an improper description of the PES with the current calculations, since the energy of the fundamental band was well reproduced (≈ 3 cm^{-1} of difference with respect to experiment). The same error is observed with respect to the CCSD(T)/ANO results for the states involving this mode, which suggests a better reproduction of the PES at this level of theory. However, in absence of the raw *ab initio* results, it is not possible to further validate this remark. A significant difference is also observed between B3LYP/SNSD and CCSD(T)/ANO results for the transition energy to $|\,1_8 2_1\,\rangle$, in strong contrast with the overall good agreement for the other modes. The most plausible explanation would be an error in the reported energy in Ref.,[84] which could be in reality 7698 cm^{-1}.

Regarding intensities, the interpretation of the result is more complex. If the comparison is done on the order of magnitude of the different peaks, the agreement between the present results and the data reported in Ref.[84] is very satisfactory. For a more quantitative analysis, only the computed CCSD(T)/ANO intensities, reported in Table 3, can be used. The difference between the two sets of theoretical values vary significantly from one transition to another, which may be associated to several origins. First of all, and contrary to what was done for the transition wavenumbers, no correction scheme was applied to the intensities, which means a major dependence on the accuracy of the electronic structure calculation regarding the definition of both potential energy and property surfaces. Moreover, as mentioned above, the numerical differentiations to obtain the anharmonic terms are done along the mass-weighted normal coordinates and the resulting derivatives must be converted to the dimensionless normal coordinates. This conversion involves the harmonic frequencies and their quality will have a direct impact on k_{ijk}, k_{ijkl}, $\boldsymbol{P}_{ij}$ and $\boldsymbol{P}_{ijk}$, hence the transition

moments. For this reason, and since the electronic structure calculations are significantly different, a quantitative comparison of the intensities is rather complex and would require an extensive benchmark, which is beyond the scope of the present work of implementation. Since a quantitative comparison with experiment is not possible, a more meaningful analysis is to compare directly the simulated spectra with their experimental counterpart. The IR spectra computed at both harmonic and anharmonic levels are shown in Fig. 2, together with the experimental one, measured over the 2000–8000 cm^{-1} wavenumber range.[97] In order to simulate the band broadening observed in the recorded spectra, Lorentzian distribution functions with half-widths at half-maximum of 12 cm^{-1} were used. The agreement with experiment appears very good but most features are hardly visible due to the low intensity of many bands with respect to the fundamental one (transition to $|\, 1_1 \,\rangle$). A zoom on the lower section of the spectra is shown in Fig. 3, together with a proposal of assignment for the visible experimental bands when the computed data are unambiguous. The assignment presented here is in agreement with the one given in Ref.,[84] which is however limited to only a few bands. The only discrepancy is for the band at about 4750 cm^{-1} (transition to $|\, 2_2 1_3 \,\rangle$). While the band position is correctly calculated at the B3LYP/SNSD level with the correction scheme, its intensity is very low, preventing a clear assignment of this band.

Naphthalene As a second example, naphthalene (Fig. 1) is a polycyclic aromatic hydrocarbon (PAH), a family of compounds considered to be significant contributors to the IR spectra registered in the interstellar medium and partly responsible for the observed aromatic infrared bands, either as isolated molecules or embedded in more complex systems (see Refs.[98,99] for more details). As the smallest member of this family, naphthalene has been extensively studied experimentally and theoretically both in its neutral and ionic forms.[74,78,79,98,100–105] In order to get a thorough characterization of the IR spectrum of such compounds, high-resolution (in the far infrared)[103–105] and near-infrared spectra[74,79] have been recorded. The latter are of interest in the present work. The same computational

procedure has been used here. The harmonic and anharmonic wavenumbers of the 48 modes of naphthalene are reported in Table 4, and compared to experimental results taken from Ref.[102] With respect to experimental frequencies, a very good agreement is found, with a mean absolute error of 5.4 cm^{-1}.

To simulate the spectra, the same fitting procedure as for nitric acid has been employed. For the 4 modes, which are both Raman and IR inactive, the shift to be applied to the harmonic part of the transition energies was assumed null. The harmonic and anharmonic spectra computed this way are reported in Table 4 together with their experimental counterpart taken from Ref.[106] As a first remark, while one would expect strong 1-1 resonances in the anharmonic transition integrals associated to the C-H stretchings fundamental bands due to the presence of near-degenerate frequencies (in particular, $\omega_1 \approx \omega_{29}$, and $\omega_2 \approx \omega_{30}$), those terms give no contribution, so the influence of the threshold $\Delta_\omega^{1\text{-}1}$ (provided it remains small) is null. The reasons for this can be found from an analysis of eq. 22. First of all, 1-1 resonances appear in the terms deriving purely from the mechanical anharmonicity (cubic, quartic and Coriolis terms). In the case where modes i and j have approximately the same energy ($\omega_i \approx \omega_j$), the transition intensity of a fundamental band associated to mode i will be impacted by a singularity if the first derivative of the property with respect to mode j ($\boldsymbol{P}_j$) is not null and there is a strong coupling between mode i and j (in k_{ijkk} and k_{ijk}) or they have both significant couplings with the same modes (in $k_{ikl}k_{jkl}$ and $\zeta_{ik}\zeta_{jk}$). In the present case, for each couple of near-degenerate modes, the first derivative of the electric dipole with respect to one of the modes is negligible while the second mode is insufficiently coupled with the other modes.

The very good agreement between the anharmonic and experimental spectra allows for a detailed assignment of the various bands observable in the latter and summarized in Fig. 5. The most intense bands in the 0–3500 cm^{-1} region are also reported in Table 5. As expected, the 3-quanta transitions are too weak to contribute in this region and most features are related to fundamental bands. An exception is the 1700–2000 cm^{-1} zone, empty in the

harmonic spectrum since it involves 2-quanta transitions but correctly represented at the anharmonic level, both for the bands positions and shapes (Fig. 4).

For higher quanta and with a medium-size system like naphthalene, a quantitative comparison of experimental and computed data is far from straightforward. The main issue is that most bands are the result of multiple contributions, which must be unraveled by mean of mathematical models. The latter generally require a preliminary hypothesis on the structure of the band and the extrapolation is often based on a local-mode theory with the coupling between the modes assumed negligible. However, as can be seen in Table 6, the main contributions in the 2-quanta and 3-quanta regions of the theoretical spectrum are related here to combination bands, incompatible with the local-mode results extrapolated from experimental data. For this reason, comparison with experiment will focus on the direct comparison with the band-shape, taken from Ref.[79] for both regions. First of all, the two experimental spectra were not registered at the same temperature, the 2-quanta region at 300 K and the 3-quanta one at 330 K, which means that some discrepancies are expected with the theoretical spectra, where hot-bands are neglected. The second and third overtones regions are shown in Fig. 6, with the most intense transitions given in Table 6. The intensities of the experimental spectra where scaled to match the computed band-shapes. For the 2-quanta region, the experimental spectrum was shifted by +85 cm^{-1}. The overall agreement with experiment is good with the different features correctly reproduced in the theoretical band-shape. As expected, this region is dominated by 2-quanta transitions but 3-quanta transitions can also be clearly identified in the right-wing of the band, in particular the small band at about 6200 cm^{-1}. However, the mixing between the CH stretching modes results in a significant number of combination states with comparable transition intensities, which prevent a clear assignment of the observed bands. It is likely related to the underlying Cartesian-based description used for the definition of the normal modes and a simpler picture should be expected by using internal coordinates. However, such a step requires further work regarding the correct description of the system and the adaptation of the equations presented

here, which are beyond the scope of this work. For the 3-quanta region, the experimental band needs to be further shifted, by a total of about 275 cm^{-1}. In this zone, the recorded spectrum shows a single band, which can be matched by using larger broadening functions with half-widths at half-maximum of 32 cm^{-1}. As for 2-quanta, the theoretical band-shape is composed of a multiple transitions of similar intensities, with the main ones reported in Table 6.

Isobutene The NIR spectrum of isobutene, or 2-methylpropene (Fig. 1), starting from the second overtone C–H stretching region has been recently recorded and analyzed with a local mode model.[80] Following the same protocol as for the previous systems, the computed harmonic and anharmonic fundamental wavenumbers are reported in Table 7 together with their experimental counterparts. Regarding the latter, it should be noted that relatively large differences can be observed in the sets used in the literature (see for instance Refs.[107–109] and references therein). The choice made here was to use the values reported in a relatively recent work by Krimm and coworkers.[109] With respect to naphthalene, the mean absolute error is higher, at about 12 cm^{-1}, on par with the nitric acid but with stronger discrepancies for some modes. In particular, the sequence of normal modes, ordered by increasing energies, is changed between the experimental and computed values. In order to be consistent with the previous studies, the fitting scheme will be kept here as well.

The simulated harmonic and anharmonic spectra obtained with the corrected energies are reported in Fig.7 and compared to their experimental counterpart.[106] As for naphthalene, it is interesting to start with a more technical discussion on the actual calculation of the transition moments, in connection with the problem of resonances. The symmetric and antisymmetric CH stretchings of CH_2 (noted CH_o for the olefinic CH vibrations in Ref.[80]) are well separated in energy with a shift of about 80 cm^{-1}. This is not the case for those of the methyl group (CH_{ip} for the vibrations where the largest displacements are in the C-C=C planes and CH_{op} for those out-of-planes, respectively modes 2 and 23 and 11 and 16 here),

with about 2 cm^{-1} of difference between the symmetric and antisymmetric modes. Due to the presence of those near-degenerate frequencies ($\omega_2 \approx \omega_{23}$, and $\omega_{11} \approx \omega_{16}$), it is expected that strong 1-1 resonances in the anharmonic transition integrals occur. However, those terms give no contribution, so the influence of the threshold $\Delta_{\omega}^{1\text{-}1}$ is null. The reasons for this are the null first derivative of the electric dipole with respect to q_{11} as shown in Table 7, while symmetry considerations prevent the necessary couplings for the other modes. As a result, even with nearly equal frequencies, there is no singularity in this case.

In the region of interest here (0-3500 cm^{-1}), fundamental bands are largely dominating. However, at variance with naphthalene, 3-quanta transitions give visible contributions in the 2900–3500 cm^{-1} zone, resulting in bands not present in the experimental spectrum. While being a potential case of 1-3 resonances, modifying the threshold $\Delta_{\omega}^{1\text{-}3}$ used to identify resonant terms has a marginal impact on the peak intensity. The 3 main peaks correspond to transitions to 3-modes combination bands, which involve 2 CH_3 torsion mode (v_{15} and v_{21}) and 1 CH stretching band of CH_3 (respectively v_{24} at 3187 cm^{-1}, v_2 at 3286 cm^{-1} and v_{11} at 3319 cm^{-1}). The cause of those peaks could be an inaccurate representation of the couplings between the normal modes based on Cartesian coordinates. An overall good agreement can be observed between the anharmonic and experimental spectra, also for the band intensities, with the main discrepancy related to the band at 880 cm^{-1}, strongly underestimated in the theoretical spectra. The shifted transitions allow for an unequivocal assignment of most bands, given in Fig. 8. It is thus possible to assign two bands to 2-quanta transitions, at about 1660 and 1750 cm^{-1}. Additional information on the contributions of the transitions to the band shape are provided in Table 8.

The 2nd and 3rd overtone regions of the IR spectrum of isobutene are shown in Fig. 9 with the most intense transitions in each region reported in Table 9. As a first remark, due to the energy of the corresponding transitions, the problem of 1-3 resonances, raised in the fundamental region, is non-existent here. For the 2-quanta region, the experimental spectrum was taken from Ref.[110] and scaled based on its most intense peak to match the computed

one. The peaks above 5750 cm^{-1} are present in both experimental and anharmonic spectra and a tentative assignment could be employed, using the data from Table 9. Nevertheless, some discrepancies regarding their relative intensities can be observed, which result in only a qualitative agreement of the computed band-shape with the experimental one. This is not the case below 5750 cm^{-1} where the features are missing in the theoretical spectrum. The reason for this discrepancy could be an insufficient accuracy of the PES, which is only marginally corrected with the fitting procedure employed here, but this may also be due to intrinsic limitations of the normal modes based on Cartesian coordinates. For the 3-quanta region, the experimental spectrum from Ref.[80] had to be shifted by about 150 cm^{-1} in order to be superimposed with the computed one. The most striking difference between the two band-shapes is their width, with the theoretical one being narrower. Because of its structure, this cannot be compensated by using a larger half-width at half-maximum to simulate the broadening. However, if this issue is set aside, an analysis of the band pattern shows similarities, albeit insufficient to permit any reliable assignment. Calculations were also performed with the polarizable continuum model (PCM) through its integral equation formalism version (IEF-PCM)[111,112] to simulate the solvent effects (xenon). However, as expected and previously noted in Ref.,[80] those effects are negligible.

Conclusions

This paper presents general and easily implementable formulas to compute fully anharmonic transitions from the ground state up to 3-quanta states within the VPT2 model. The possibility of calculating 3-quanta transitions presents an interest when investigating near-infrared spectra up to the second overtone region. Moreover, it can lead to a better description of sensitive spectroscopies, like vibrational circular dichroism. The preliminary results obtained with naphthalene and isobutene are encouraging, with the possibility to represent meaningfully the band-shape in the 9000 cm^{-1} region. It is expected that more

demanding computations involving electronic structure calculations at higher levels of theory should be able to further improve the accuracy of the theoretical spectra. This would also give the possibility to assess systematically the reliability of VPT2 for 3-quanta calculations. Finally, the contributions from the 3-quanta transitions in the IR region below 3500 cm^{-1} of isobutene due to the couplings between CH stretchings from the CH_2 groups with the methylic torsions hints at the likely necessity for a better description of the vibrations by using internal coordinates instead of the Cartesian ones.

Future works are planned to investigate the possibilities offered by this machinery for other spectroscopies, especially those mentioned above (VCD, Raman), on more diverse molecular systems.

Acknowledgement

The author is very grateful to prof. Vincenzo Barone and Dr. Małgorzata Biczysko for the helpful discussions and their suggestions in this work. Financial support form the Italian MIUR (FIRB 2012: "Progettazione di materiali nanoeterogenei per la conversione di energia solare", prot.: RBFR122HFZ and PRIN 2012,"STAR: Spettroscopia e Tecniche computazionali per la ricerca Astrofisica, atmosferica e Radioastronomica", prot.: 20129ZFHFE). Support from Gaussian, Inc. is greatly appreciated.
The high performance computer facilities of the DREAMS center (http://dreamshpc.sns.it) are acknowledged for providing computer resources.

Table 2: Harmonic (ω) and anharmonic (ν) wavenumbers (in cm^{-1}) for the modes of nitric acid. The superscript "$*$" indicates that a variational treatment was applied to the anharmonic frequencies due to the presence of Fermi resonances. Experimental wavenumbers are taken from ref.[83] ("A" stands for asymmetric and "S" for symmetric, "ip" for in-plane, "op" for out-of plane). Δ_i represents the error of anharmonic frequencies with respect to experimental data and MAE the mean absolute error.

	Symm	Mode	ω	ν	Exp.	Δ_i
1	A'	O–H str.	3719.586	3535.822	3550.7	14.878
2		NO_2 str. (A)	1768.847	1725.108	1709.568	-15.540
3		NO_2 str. (S)	1360.312	1329.958	1326.185	-3.773
4		H–ON bend.	1329.226	1299.552*	1303.069	3.517
5		NO_2 bend. (ip)	905.071	881.651	879.109	-2.542
6		O–NO_2 str.	655.219	639.572	646.826	7.254
7		O–NO_2 bend.	589.835	577.343	580.304	2.961
8	A''	NO_2 bend. (op)	775.522	763.040	763.154	0.114
9		O–H torsion	488.010	445.286	458.229	12.943
				MAE	7.058	

Table 3: Harmonic (ω), anharmonic (ν) wavenumbers (in cm^{-1}) and the corresponding CCSD(T)/ANO (ν_{CC}) or experimental (Exp.) values from Ref.[84] ν^{corr} are the anharmonic frequencies obtained by correcting the harmonic part so that the fundamental frequencies are equal to their experimental counterparts. The anharmonic (I^{anh}) and CCSD(T)/ANO (I^{CC}) are in cm molecule^{-1}. MAE stands for the mean absolute error of the corrected anharmonic wavenumbers (ν^{corr}) with respect to the values given in the column in which the MAE value is printed.

Final state	ω	ν	ν^{corr}	ν_{CC}	Exp.	I_{anh}	I_{CC}
$\vert 2_9 \rangle$	976.02	856.865	882.751		896.448	6.58×10^{-19}	
$\vert 3_9 \rangle$	1464.03	1234.738	1273.567		1288.84	2.44×10^{-20}	
$\vert 2_4 \rangle$	2658.452	2563.935	2570.969		2530.1	3.91×10^{-19}	
$\vert 2_3 \rangle$	2720.624	2651.298	2643.752		2644.4	3.18×10^{-19}	
$\vert 1_1 \rangle$	3719.586	3535.822	3550.7		3550.7	1.37×10^{-17}	1.21×-17
$\vert 3_4 \rangle$	3987.679	3829.473	3840.024		3862.4	4.23×10^{-21}	
$\vert 1_9 1_1 \rangle$	4207.597	3974.367	4002.188	4004.4	4006	2.45×10^{-19}	2.18×-19
$\vert 1_7 1_1 \rangle$	4309.421	4109.517	4127.356	4127.4	4127	5.18×10^{-20}	4.23×-20
$\vert 1_6 1_1 \rangle$	4374.806	4175.487	4197.619	4197	4195	5.41×10^{-21}	6.93×-21
$\vert 1_8 1_1 \rangle$	4495.109	4298.848	4313.84	4313.9		1.48×10^{-21}	5.69×-22
$\vert 1_5 1_1 \rangle$	4624.658	4418.63	4430.966	4430	4440	2.04×10^{-20}	3.04×-20
$\vert 1_4 1_1 \rangle$	5048.813	4795.043	4813.438	4833	4831	1.38×10^{-19}	7.24×-20
$\vert 1_3 1_1 \rangle$	5079.899	4861.676	4872.781	4864.3	4866	8.15×10^{-20}	1.62×-19
$\vert 1_2 1_1 \rangle$	5488.434	5256.621	5255.959	5255.1	5254.2	8.07×10^{-20}	8.10×-20
$\vert 2_4 1_1 \rangle$	6378.039	6043.312	6065.224		6139	1.12×10^{-22}	
$\vert 2_1 \rangle$	7439.173	6910.774	6940.53	6935	6940	6.89×10^{-19}	6.17×-19
$\vert 1_9 2_1 \rangle$	7927.183	7342.579	7385.278	7384	7381.1	9.79×10^{-21}	8.15×-21
$\vert 1_7 2_1 \rangle$	8029.007	7480.821	7513.538	7507.9		2.15×10^{-21}	5.94×-22
$\vert 1_6 2_1 \rangle$	8094.392	7550.532	7587.542	7580.9		2.22×10^{-22}	1.28×-22
$\vert 1_8 2_1 \rangle$	8214.695	7673.787	7703.657	7598		9.68×10^{-23}	5.81×-23
$\vert 1_5 2_1 \rangle$	8344.244	7794.739	7821.953	7814.7		1.97×10^{-22}	1.96×-22
$\vert 1_4 2_1 \rangle$	8768.399	8141.773	8175.046	8196.4	8198	1.40×10^{-20}	4.93×-21
$\vert 1_3 2_1 \rangle$	8799.485	8232.524	8258.507	8236	8260	3.34×10^{-21}	1.03×-20
$\vert 1_2 2_1 \rangle$	9208.02	8627.264	8641.48	8634.1		2.12×10^{-21}	1.64×-21
$\vert 3_1 \rangle$	11158.759	10124.856	10169.49	10152	10173	4.50×10^{-20}	3.07×-20
			MAE	12.974	13.402		

Table 4: Harmonic (ω), anharmonic (ν) and experimental wavenumbers (in cm^{-1}) for the modes of naphthalene. The superscript "$*$" indicates that a variational treatment was applied to the anharmonic frequencies due to the presence of Fermi resonances. Experimental data were taken from Ref.[102] The description of the vibrations is roughly based on Ref.[100] ($\parallel$ for vibrations in the aromatic plan and $\perp$ for those out of the plan). Only the non-negligible components first derivatives of the electric dipole with respect to the dimensionless normal coordinates ($\boldsymbol{\mu}_i$, in Debye) are reported. MAE stands for the mean absolute error of the corrected anharmonic wavenumbers (ν) with respect to the values given in the column in which the MAE value is printed.

	Symm	Mode	ω	ν	Exp.	$\boldsymbol{\mu}_i$
1	A_g	CH stretch.	3192.8	3058.5	3057	
2		CH stretch.	3167.9	3040.3*	3051	
3		CC stretch.	1614.8	1578.7	1576	
4		CH bend. ($\parallel$)	1489.6	1462.0*	1464	
5		$C^{\gamma}C^{\gamma}$ stretch.	1411.4	1376.6	1383	
6		CH bend. ($\parallel$)	1178.8	1166.6	1168	
7		skeletal distort. ($\parallel$)	1044.0	1030.6	1025	
8		skeletal breath.	771.0	759.9	764	
9		skeletal dist. ($\parallel$)	517.9	513.1	513	
10	A_u	CH bend. ($\perp$)	997.4	961.0		
11		CH bend. ($\perp$)	850.9	828.9		
12		skeletal distort. ($\perp$)	634.0	614.9		
13		skeletal distort. ($\perp$)	186.1	179.1		
14	B_{1g}	CH bend. ($\perp$)	965.2	935.6	952	
15		CH bend. ($\perp$)	731.4	713.4	726	
16		skeletal distort. ($\perp$)	396.8	383.9	390	
17	B_{1u}	CH stretch.	3180.2	3049.7	3065	-2.951y
18		CH stretch.	3162.4	3011.0*	3008	-1.018y
19		CC stretch.	1639.4	1603.3	1602	$4.305\times10^{-1}y$

	Symm	Mode	ω	ν	Exp.	$\boldsymbol{\mu}_i$
20		CH bend. ($\parallel$)	1415.1	1389.8	1392	$5.537\times10^{-1}y$
21		CH bend. ($\parallel$)	1285.6	1265.5*	1268	$-6.764\times10^{-1}y$
22		CC distort. ($\parallel$)	1144.8	1132.2	1130	$5.235\times10^{-1}y$
23		skeletal distort. ($\parallel$)	801.9	795.9	796	$1.117\times10^{-1}y$
24		skeletal distort. ($\parallel$)	363.2	362.3	359	$1.785\times10^{-1}y$
25	B_{2g}	CH bend. ($\perp$)	1002.5	965.5	979	
26		CH bend. ($\perp$)	903.2	872.2	880	
27		skeletal distort. ($\perp$)	796.3	734.9	773	
28		skeletal distort. ($\perp$)	482.2	466.7	465	
29	B_{2u}	CH stretch.	3192.0	3056.2*	3057	$-2.546x$
30		CH stretch.	3164.6	3037.4*	3042	$-3.324\times10^{-1}x$
31		CC stretch.	1548.3	1512.5*	1514	$7.970\times10^{-1}x$
32		CC stretch.	1399.4	1371.1*	1361	$1.574\times10^{-1}x$
33		CH bend. ($\parallel$)	1232.9	1216.5	1210	$-2.129\times10^{-1}x$
34		CH bend. ($\parallel$)	1169.4	1153.2	1135	$1.836\times10^{-1}x$
35		skeletal breath.	1033.9	1017.2	1012	$7.090\times10^{-1}x$
36		skeletal distort. ($\parallel$)	629.0	624.2	620	$3.303\times10^{-1}x$
37	B_{3g}	CH stretch.	3179.1	3055.1*	3057	
38		CH stretch.	3160.6	3015.5*	3018	
39		CC stretch.	1672.0	1629.9	1629	
40		CC stretch.	1488.8	1461.0*	1458	
41		CH bend. ($\parallel$)	1266.5	1244.4	1240	
42		CH bend. ($\parallel$)	1167.7	1150.3	1145	
43		skeletal distort. ($\parallel$)	942.2	934.9	936	
44		skeletal distort. ($\parallel$)	514.8	509.6	509	
45	B_{3u}	CH bend. ($\perp$)	986.0	956.2	959	$4.448\times10^{-1}z$

Symm	Mode	ω	ν	Exp.	$\boldsymbol{\mu}_i$
46	CH bend. ($\perp$)	803.0	779.8	782	$2.272z$
47	CC distort. ($\perp$)	492.9	474.0	473	$7.949\times10^{-1}z$
48	Ring wag.	173.6	167.7	166	$1.549\times10^{-1}z$
			MAE	5.4	

Table 5: Highest harmonic ($I_{\mathbf{harm}}$) and anharmonic ($I_{\mathbf{anh}}$) transition intensities (in km/mol) of the IR spectrum of naphthalene in the 0–3500 cm^{-1} region. Transition energies (both harmonic, ω, and anharmonic, ν) are given in cm^{-1}.

Final state	ω	ν	ν^{corr}	I_{harm}	I_{anh}
$\vert\, 1_{47}\,\rangle$	492.9	474.0	473.0	23.29	19.42
$\vert\, 1_{36}\,\rangle$	629.0	624.2	620.0	3.15	3.09
$\vert\, 1_{46}\,\rangle$	803.0	779.8	782.0	116.78	110.18
$\vert\, 1_{45}\,\rangle$	986.0	956.2	959.0	3.65	4.04
$\vert\, 1_{35}\,\rangle$	1033.9	1017.2	1012.0	8.83	8.34
$\vert\, 1_{21}\,\rangle$	1285.6	1265.5	1268.0	6.47	6.20
$\vert\, 1_{20}\,\rangle$	1415.1	1389.8	1392.0	3.94	3.11
$\vert\, 1_{31}\,\rangle$	1548.3	1512.5	1514.0	7.45	7.47
$\vert\, 1_{10}1_{25}\,\rangle$	1999.9	1919.0	1932.5		3.26
$\vert\, 1_{18}\,\rangle$	3162.4	3011.0	3008.0	5.96	4.79
$\vert\, 1_{17}\,\rangle$	3180.2	3049.7	3065.0	49.76	66.99
$\vert\, 1_{29}\,\rangle$	3192.0	3056.2	3057.0	36.91	48.54

Table 6: Highest anharmonic (I) transition intensities (in km/mol) of the IR spectrum of naphthalene in the 2nd and 3rd overtone regions. Transition energies (both harmonic, ω, and anharmonic, ν) are given in cm^{-1}.

Final state	ω	ν	ν^{corr}	I
$\vert\, 1_{18}1_{38}\,\rangle$	6323.0	6024.8	6024.3	0.875
$\vert\, 1_{30}1_{38}\,\rangle$	6325.2	6035.2	6042.3	1.800
$\vert\, 1_{2}1_{18}\,\rangle$	6330.3	6036.2	6043.9	1.352
$\vert\, 1_{17}1_{38}\,\rangle$	6340.7	6052.1	6069.9	0.512
$\vert\, 1_{18}1_{37}\,\rangle$	6341.5	6053.7	6052.6	0.888
$\vert\, 1_{17}1_{37}\,\rangle$	6359.3	6075.4	6092.6	0.996
$\vert\, 1_{1}1_{29}\,\rangle$	6384.8	6076.2	6075.5	0.688
$\vert\, 1_{1}1_{17}1_{37}\,\rangle$	9552.1	9065.3	9081.0	0.075
$\vert\, 1_{1}1_{18}1_{37}\,\rangle$	9534.3	9049.7	9047.1	0.063
$\vert\, 1_{2}1_{30}1_{37}\,\rangle$	9511.6	9053.1	9070.3	0.062
$\vert\, 1_{2}1_{30}1_{38}\,\rangle$	9493.0	8997.4	9015.2	0.100
$\vert\, 1_{18}1_{37}1_{38}\,\rangle$	9502.1	9027.8	9029.2	0.057

Table 7: Harmonic (ω), anharmonic (ν) and experimental wavenumbers (in cm^{-1}) for the modes of isobutene. The superscript "$*$" indicates that a variational treatment was applied to the anharmonic frequencies due to the presence of Fermi resonances. The description of the vibrations is based on Ref.[107] (A stands for asymmetric and S for symmetric). Only the non-negligible components first derivatives of the electric dipole with respect to the dimensionless normal coordinates ($\boldsymbol{\mu}_i$, in Debye) are reported. MAE stands for the mean absolute error of the corrected anharmonic wavenumbers (ν) with respect to the values given in the column in which the MAE value is printed.

	Symm	Mode	ω	ν	Exp.	$\boldsymbol{\mu}_i$
1	A_1	CH str. of CH_2 (S)	3132.8	2987.5*	2989	$1.203y$
2		CH str. of CH_3 (A)	3106.3	2962.7	2941	$-1.880y$
3		CH str. of CH_3 (S)	3012.3	2926.6*	2911	$-2.657y$
4		C=C str.	1714.0	1668.5*	1661	$1.487y$
5		CH_3 def. (A)	1496.2	1456.3	1470	$1.108y$
6		CH_2 def	1439.1	1412.7*	1416	$-3.047\times10^{-1}y$
7		CH_3 def. (S)	1406.8	1378.9*	1366	$-1.141\times10^{-1}y$
8		CH_3 rock	1078.7	1057.6	1064	$-4.031\times10^{-1}y$
9		C–C str. (S)	815.3	798.3	801	$8.982\times10^{-2}y$
10		skeletal def.	378.7	380.9	383	$7.789\times10^{-2}y$
11	A_2	CH str. of CH_3 (A)	3052.6	2912.7	2970	
12		CH_3 def. (A)	1464.6	1429.3	1450	
13		CH_3 rock.	1013.2	991.6	988	
14		CH_2 tors.	699.8	682.6	700	
15		CH_3 tors.	173.7	163.0	165	
16	B_1	CH str. of CH_3 (A)	3055.1	2914.7	2945	$-2.641z$
17		CH_3 def. (A)	1482.7	1436.2*	1444	$1.134z$
18		CH_3 rock.	1099.2	1074.4	1079	$-1.061\times10^{-1}z$
19		CH_2 wag	914.2	888.1	890	$1.539z$
20		skeletal wag	440.2	439.9	429	$4.550\times10^{-1}z$
21		CH_3 tors.	210.3	196.0	196	$-6.861\times10^{-2}z$
22	B_2	CH str. of CH_2 (A)	3213.1	3070.0	3086	$1.792x$
23		CH str. of CH_3 (A)	3104.4	2964.0*	2980	$2.114x$
24		CH str. of CH_3 (S)	3006.9	2921.5*	2893	$-1.789x$
25		CH_3 def. (A)	1477.7	1447.8*	1458	$-5.548\times10^{-1}x$
26		CH_3 def. (S)	1404.6	1370.9	1381	$-8.335\times10^{-1}x$
27		C–C str. (A)	1293.6	1264.4	1282	$-4.482\times10^{-1}x$
28		CH_2 rock.	982.3	963.7	974	$1.779\times10^{-1}x$
29		CH_3 rock.	956.6	942.9	950	$2.173\times10^{-2}x$
30		skeletal rock.	435.8	437.3	430	$2.019\times10^{-1}x$
				MAE	12.2	

Table 8: Highest harmonic ($I_{\mathbf{harm}}$) and anharmonic ($I_{\mathbf{anh}}$) transition intensities (in km/mol) of the IR spectrum of isobutene in the 0–3500 cm^{-1} region. Transition energies (both harmonic, ω, and anharmonic, ν) are given in cm^{-1}.

Final state	ω	ν	ν^{corr}	I_{harm}	I_{anh}
$\mid 1_{20} \rangle$	440.2	439.9	429.0	8.55	8.49
$\mid 1_{19} \rangle$	914.2	888.1	890.0	47.08	43.95
$\mid 1_{26} \rangle$	1404.6	1370.9	1381.0	8.99	8.18
$\mid 1_{17} \rangle$	1482.7	1436.2	1444.0	15.74	11.94
$\mid 1_{5} \rangle$	1496.2	1456.3	1470.0	14.90	14.29
$\mid 1_{4} \rangle$	1714.0	1668.5	1661.0	23.43	23.57
$\mid 1_{24} \rangle$	3006.9	2921.5	2893.0	19.35	20.21
$\mid 1_{3} \rangle$	3012.3	2926.6	2911.0	42.57	43.42
$\mid 1_{16} \rangle$	3055.1	2914.7	2945.0	41.47	45.19
$\mid 1_{23} \rangle$	3104.4	2964.0	2980.0	26.16	32.17
$\mid 1_{2} \rangle$	3106.3	2962.7	2941.0	20.68	15.85
$\mid 1_{1} \rangle$	3132.8	2987.5	2989.0	8.39	11.35
$\mid 1_{22} \rangle$	3213.1	3070.0	3086.0	18.16	22.44
$\mid 1_{11}1_{15}1_{21} \rangle$	3436.7	3260.0	3319.3		5.30

Table 9: Highest anharmonic (I) transition intensities (in km/mol) of the IR spectrum of isobutene in the 2nd and 3rd overtone regions. Transition energies (both harmonic, ω, and anharmonic, ν) are given in cm^{-1}.

Final state	ω	ν	ν^{corr}	I
$\vert\, 2_{11}\,\rangle$	6105.3	5777.6	5892.2	0.623
$\vert\, 2_{16}\,\rangle$	6110.3	5811.5	5872.1	0.738
$\vert\, 1_2 1_{23}\,\rangle$	6210.8	5834.6	5828.9	0.776
$\vert\, 1_1 1_{22}\,\rangle$	6345.9	5949.1	5966.6	0.405
$\vert\, 2_{22}\,\rangle$	6426.2	6075.5	6107.5	1.133
$\vert\, 1_3 1_{11} 1_{24}\,\rangle$	9071.9	8534.8	8548.0	0.053
$\vert\, 1_{11} 1_{16} 1_{24}\,\rangle$	9114.7	8525.6	8528.9	0.144
$\vert\, 2_2 1_{23}\,\rangle$	9317.1	8658.3	8630.9	0.052
$\vert\, 1_1 2_{22}\,\rangle$	9559.0	8839.5	8873.0	0.098

Figure 1: Skeletal formulas of isobutene (1), naphthalene (2) and nitric acid (3). For the first molecules, all carbons are in the (y,z) plan and the x axis points toward the reader. For nitric acid, all atoms are in the (x,y) plane. The "γ" symbols designates the positions of the "C$^{\gamma}$" used in the description of the vibrations in Table 4.

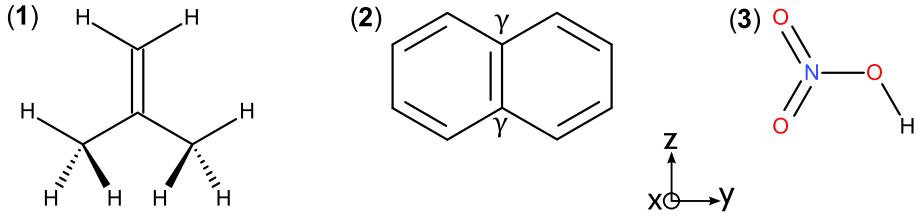

Figure 2: Simulated (harmonic and anharmonic) and experimental IR spectra of nitric acid in the 2000–8000 cm^{-1} region. The theoretical spectra were obtained by applying lorentzian distribution functions with half-widths at half-maximum of 12 cm^{-1} to account for the band broadening. Experimental data were taken from Ref.[97] The experimental spectrum was scaled to match the highest anharmonic peak.

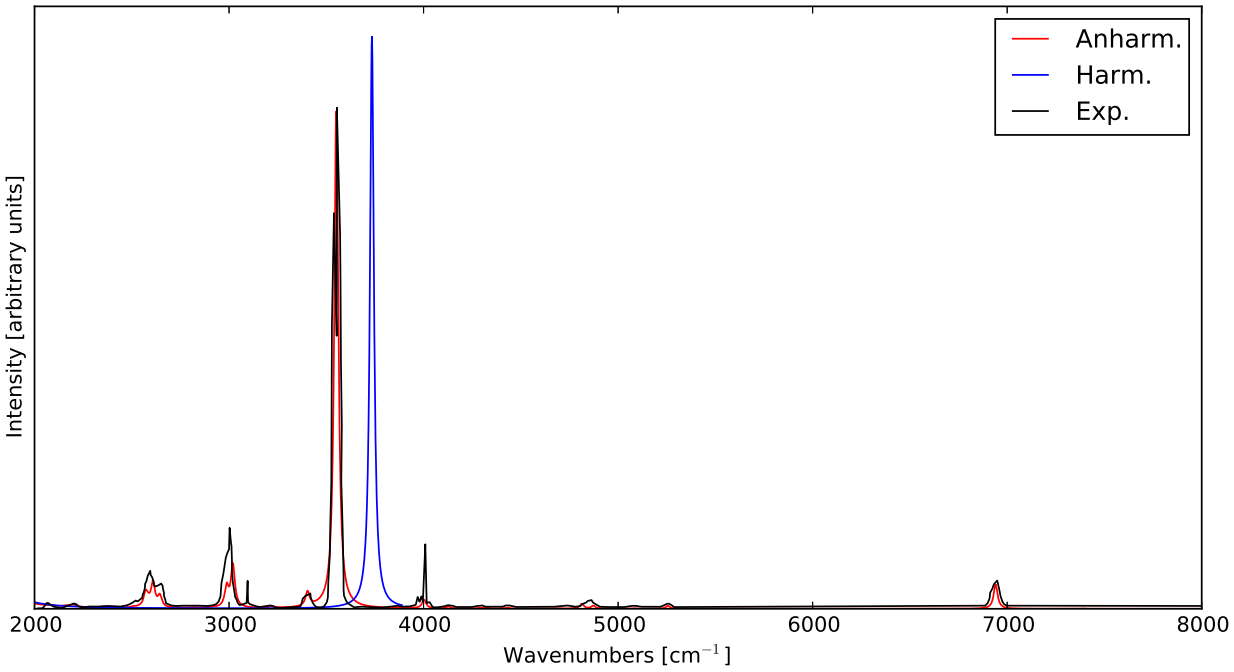

Figure 3: Simulated anharmonic and experimental IR spectra of nitric acid in the 2000–8000 cm^{-1} region. The transitions have been divided based on the total number of quanta in the final state. Experimental data were taken from Ref.[97] Since all transitions have the vibrational ground state as origin, only the final state is reported for the band assignment. Multiple significant contributions are separated by commas

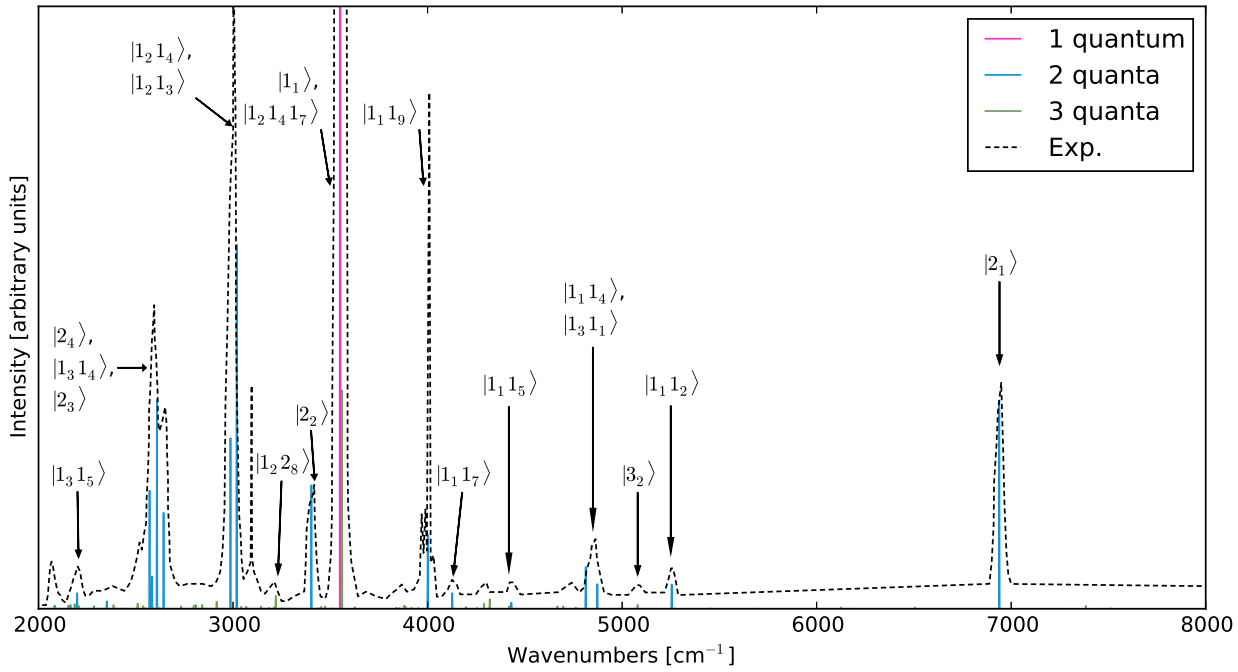

Figure 4: Simulated (harmonic and anharmonic) and experimental IR spectra of naphthalene in the 0–3500 cm^{-1} region. The theoretical spectra were obtained by applying lorentzian distribution functions with half-widths at half-maximum of 12 cm^{-1} to account for the band broadening. Experimental data were taken from Ref.[106] The experimental spectrum was scaled to match the highest anharmonic peak

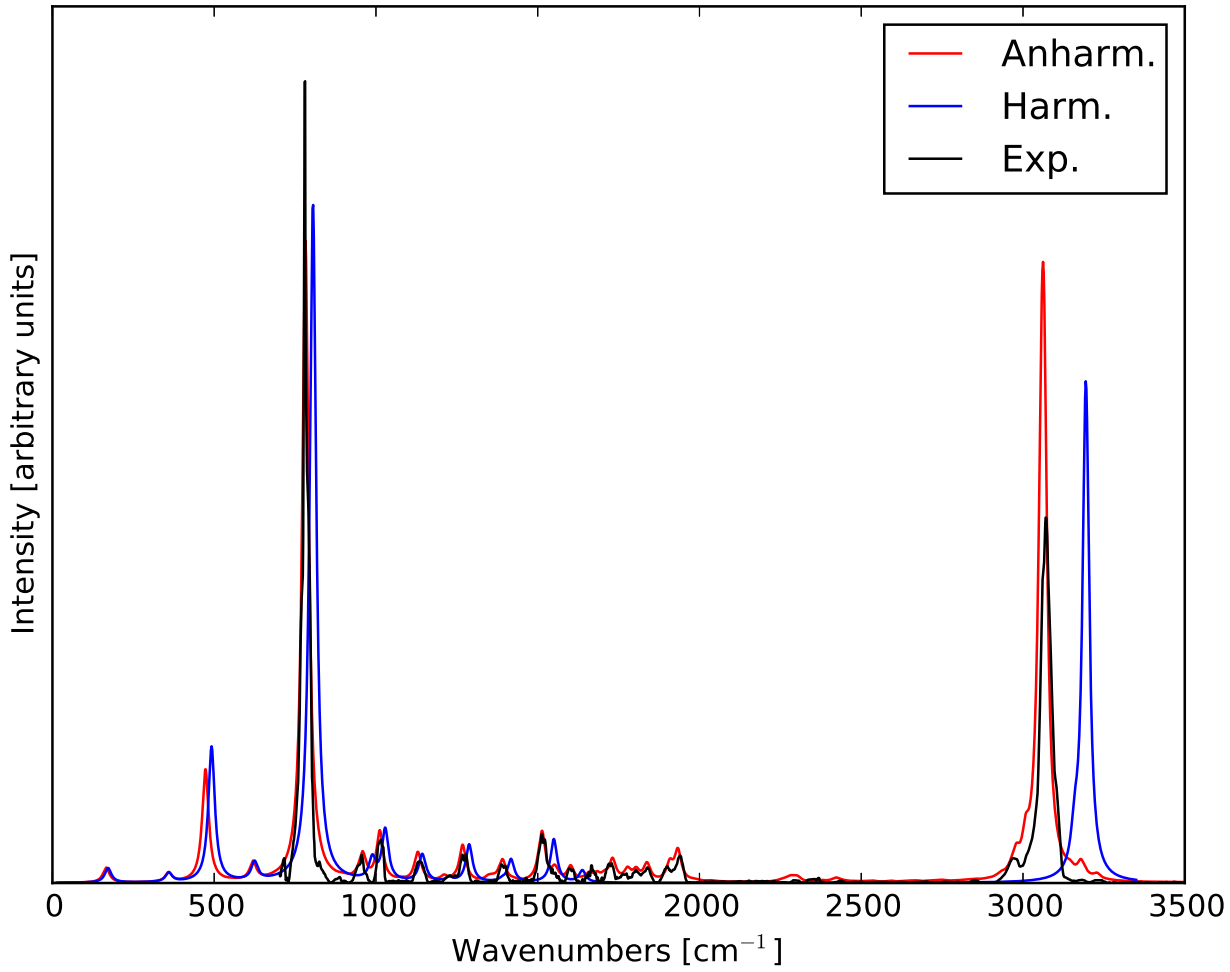

Figure 5: Simulated anharmonic and experimental IR spectra of naphthalene in the 0–3500 cm^{-1} region. The transitions have been divided based on the total number of quanta in the final state. Experimental data were taken from Ref.[106] In order to view the contributions to the smaller bands, the most intense bands have been truncated.
The letters refer to the following band assignment, where only the final state is reported (multiple contributions are indicated with a "+" sign): A: $|\,1_{46}\,\rangle$; B: $|\,1_{45}\,\rangle$; C: $|\,1_{35}\,\rangle$; D: $|\,1_{36}1_{44}\,\rangle+|\,1_{22}\,\rangle$; E: $|\,1_{21}\,\rangle$; F: $|\,1_{20}\,\rangle$; G: $|\,1_{31}\,\rangle$; H: $|\,1_{19}\,\rangle$; I: $|\,1_{26}1_{46}\,\rangle+|\,1_{15}1_{45}\,\rangle$; J: $|\,1_{14}1_{46}\,\rangle$; K: $|\,1_{11}1_{14}\,\rangle$; L: $|\,1_{11}1_{25}\,\rangle$; M: $|\,1_{26}1_{45}\,\rangle+|\,1_{10}1_{26}\,\rangle$; N: $|\,1_{14}1_{45}\,\rangle+|\,1_{10}1_{14}\,\rangle$; O: $|\,1_{10}1_{25}\,\rangle+|\,1_{25}1_{45}\,\rangle$; P: $|\,1_{32}1_{39}\,\rangle$; Q: $|\,1_{18}\,\rangle$; R: $|\,1_{17}\,\rangle+|\,1_{29}\,\rangle$; S: $|\,1_{3}1_{19}\,\rangle$; T: $|\,1_{19}1_{39}\,\rangle$

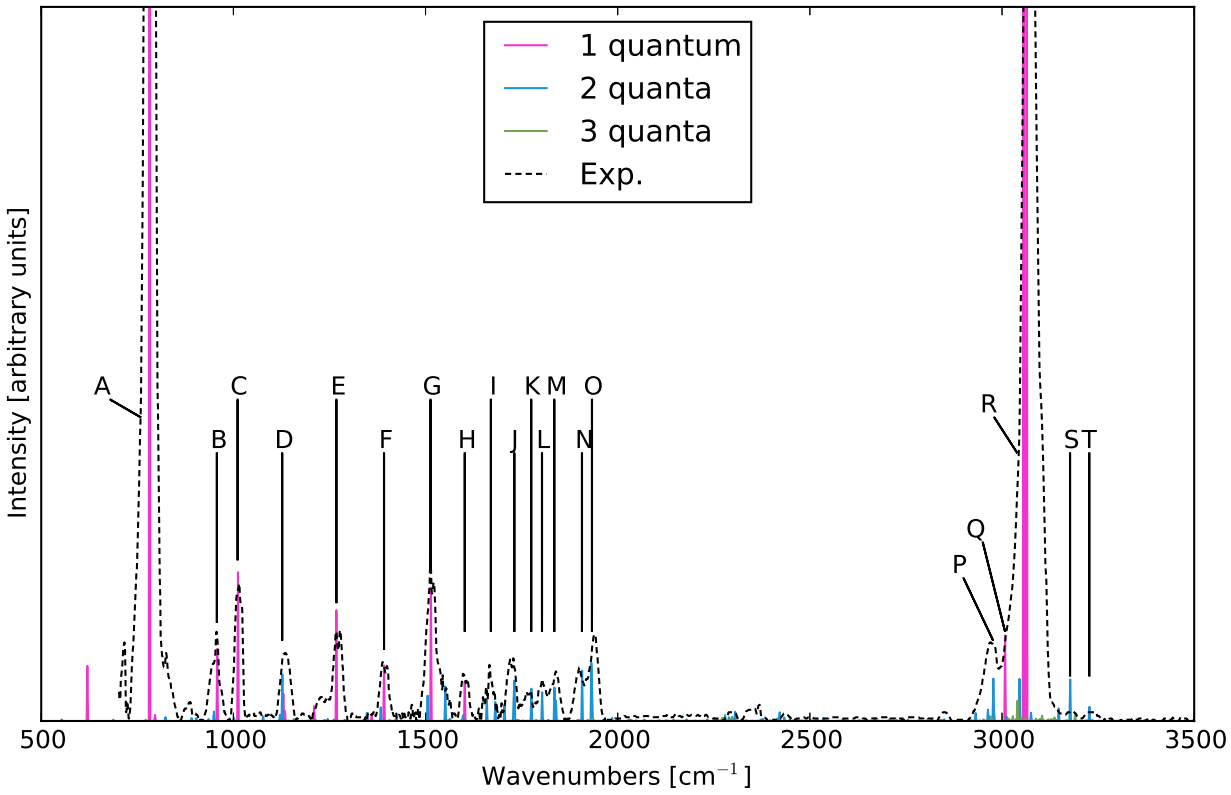

Figure 6: Simulated IR spectra of naphthalene in the 5500–6500 cm^{-1} (2nd overtone, left panel) and 8600-9500 cm^{-1} (3rd overtones, right panel) regions. Band broadening was simulated by means of lorentzian distribution functions with half-width at half-maximum of 12 cm^{-1}. For the 3-quanta region, a broadening with HWHM=32 cm^{-1} (HW32) has been also used and the band obtained with the default broadening (HW12) was scaled down by a factor of two. The transitions have been divided based on the total number of quanta in the final state. The experimental spectrum was taken from Ref.[79] and shifted by +250 cm^{-1} and scaled so that its highest peak matched the highest theoretical one.

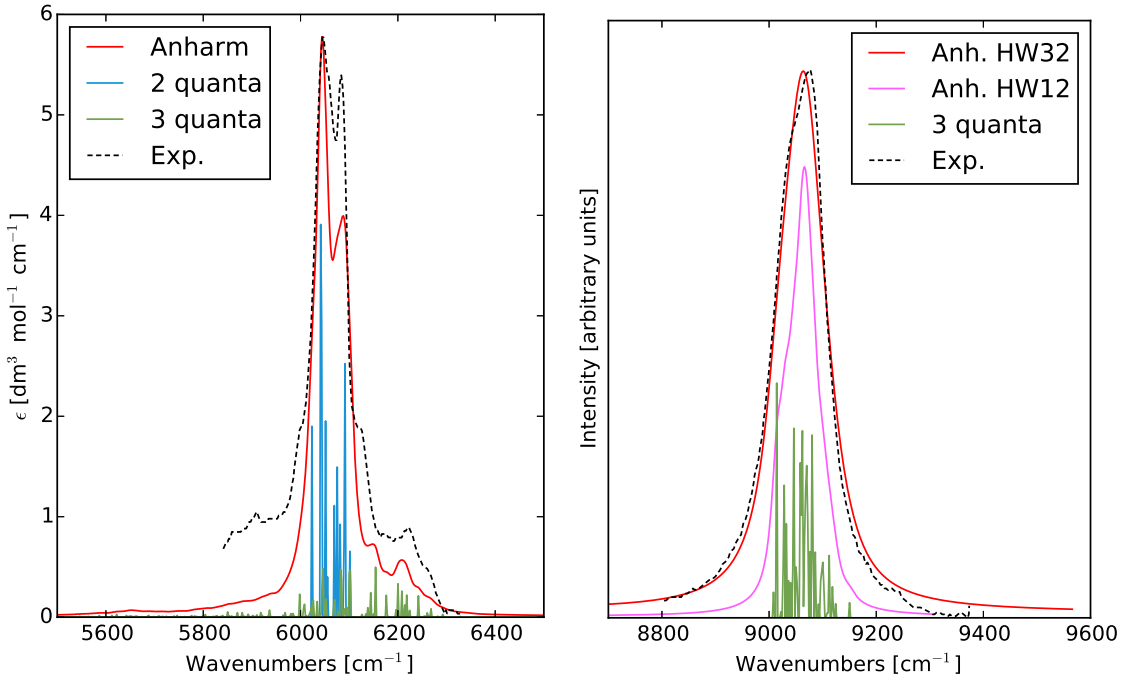

Figure 7: Simulated (harmonic and anharmonic) and experimental IR spectra of isobutene in the 0–3500 cm^{-1} region. The theoretical spectra were obtained by applying lorentzian distribution functions with half-width at half-maximum of 12 cm^{-1} to account for the band broadening. Experimental data were taken from Ref.[106] The experimental spectrum was scaled to match the highest anharmonic peak.

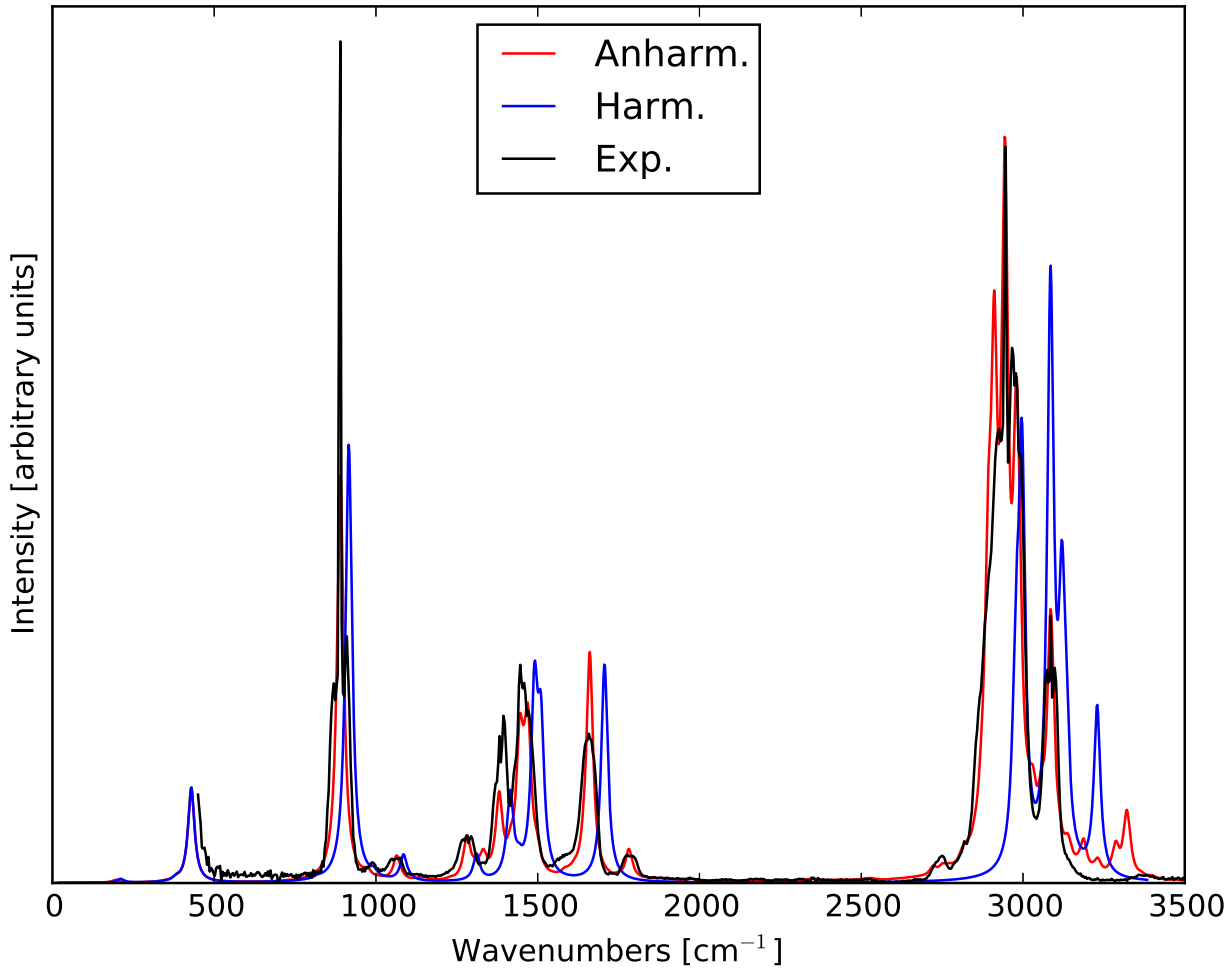

Figure 8: Simulated anharmonic and experimental IR spectra of isobutene in the 0–3500 cm^{-1} region. The transitions have been divided based on the total number of quanta in the final state. Experimental data were taken from Ref.[106]
The letters refer to the following band assignment, where only the final state is reported (multiple contributions are indicated with a "+" sign): A: $|1_{19}\rangle$; B: $|1_{28}\rangle$; C: $|1_{8}\rangle$; D: $|1_{27}\rangle$; E: $|1_{26}\rangle$; F: $|1_{17}\rangle+|1_{5}\rangle$; G: $|1_{4}\rangle$; H: $|2_{18}\rangle$; I: $|2_{7}\rangle$; J: $|1_{24}\rangle+|1_{3}\rangle$; K: $|1_{16}\rangle$; L: $|1_{23}\rangle+|1_{2}\rangle$; M: $|1_{1}\rangle$

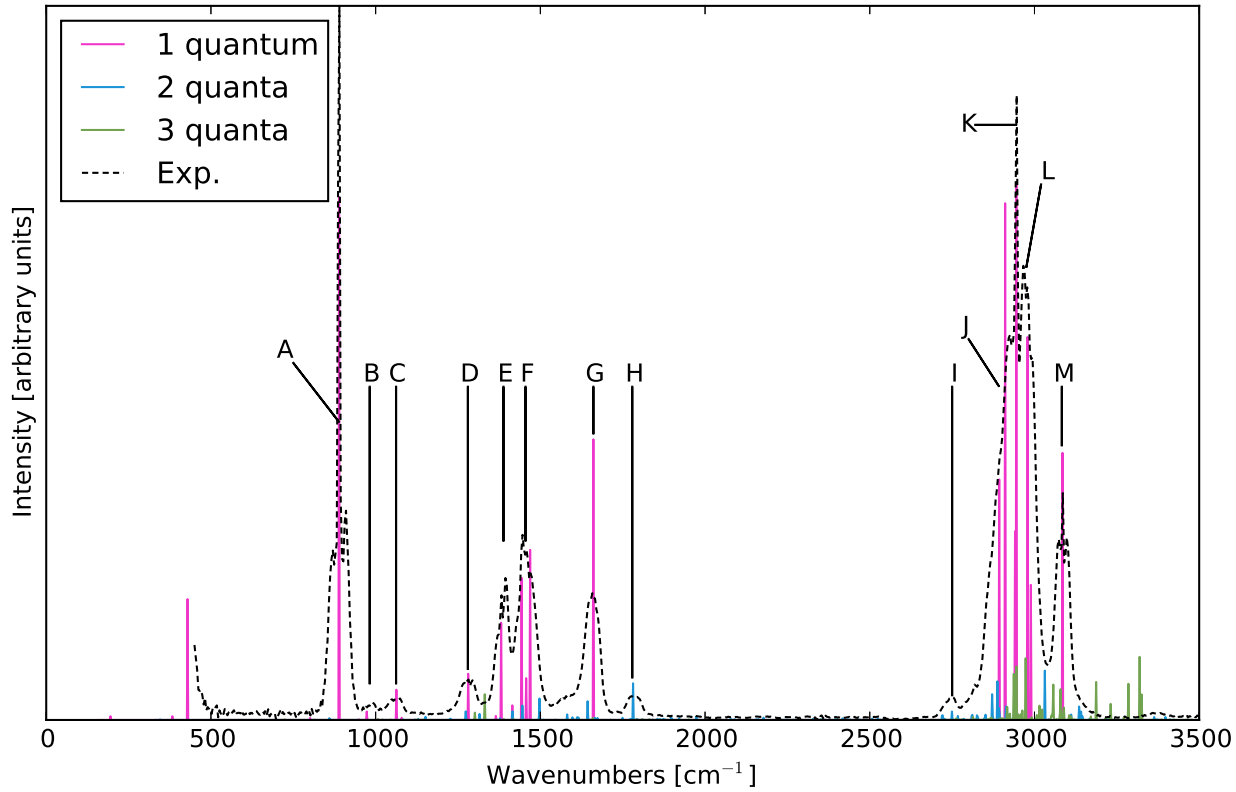

Figure 9: Simulated IR spectra of isobutene in the 5500–6500 cm^{-1} (2nd overtone, left panel) and 8200-9200 cm^{-1} (3rd overtones, right panel) regions. Band broadening was simulated by means of lorentzian distribution functions with half-width at half-maximum of 12 cm^{-1}. The transitions have been divided based on the total number of quanta in the final state. The experimental spectra were taken from Refs.[110] (left panel) and[80] (right panel) and scaled so that its highest peak matched the highest theoretical one. The latter was shifted by +150 cm^{-1}.

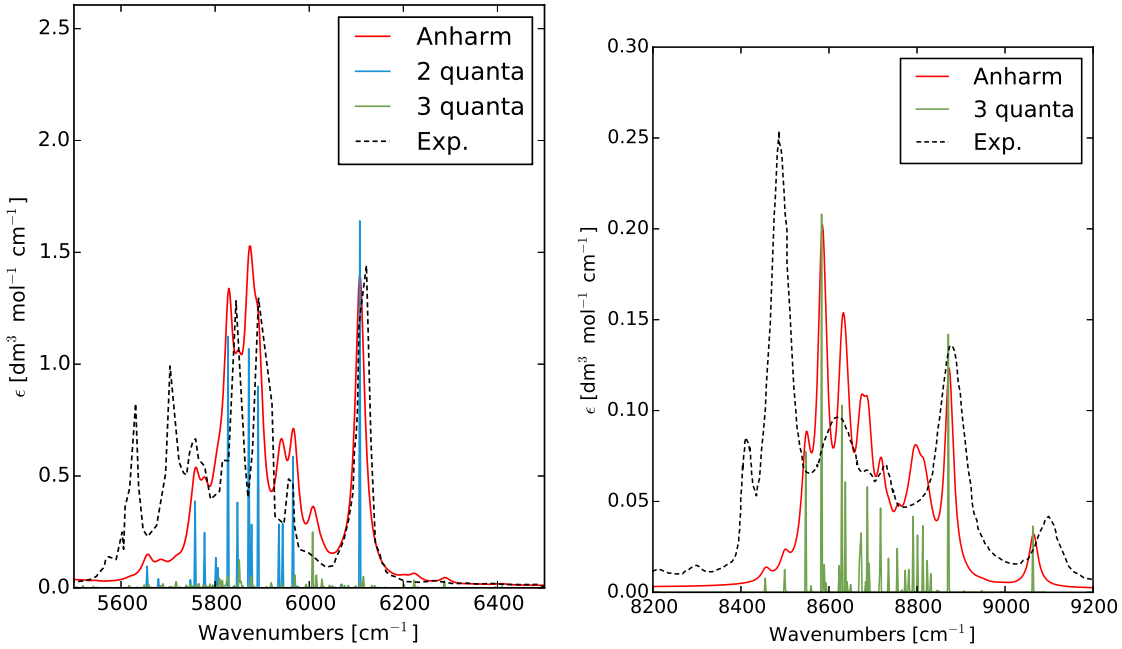

References

(1) Jensen, P.; Bunker, P. R. *Computational Molecular Spectroscopy*; John Wiley and Sons Ltd, Chichester, UK, 2000.

(2) Grunenberg, J., Ed. *Computational Spectroscopy: Methods, Experiments and Applications*; John Wiley & Sons, Inc., 2010; p 432.

(3) Barone, V., Ed. *Computational Strategies for Spectroscopy: from Small Molecules to Nano Systems*; John Wiley & Sons, Inc., 2011.

(4) Barone, V.; Baiardi, A.; Biczysko, M.; Bloino, J.; Cappelli, C.; Lipparini, F. Implementation and Validation of a Multi-Purpose Virtual Spectrometer for Large Systems in Complex Environments. *Phys. Chem. Chem. Phys.* **2012**, *14*, 12404–12422.

(5) Stanton, J. F.; Gauss, J.; Harding, M. E.; Szalay, P. G. CFour A Quantum Chemical Program Package. 2011; with contributions from A. A. Auer, R. J. Bartlett, U. Benedikt, C. Berger, D. E. Bernholdt, Y. J. Bomble, O. Christiansen, M. Heckert, O. Heun, C. Huber, T.-C. Jagau, D. Jonsson, J. Jusélius, K. Klein, W. J. Lauderdale, D. Matthews, T. Metzroth, L. A. Mueck, D. P. O'Neill, D. R. Price, E. Prochnow, C. Puzzarini, K. Ruud, F. Schiffmann, W. Schwalbach, S. Stopkowicz, A. Tajti, J. Vázquez, F. Wang, J. D. Watts and the integral packages MOLECULE (J. Almloef and P. R. Taylor), PROPS (P. R. Taylor), ABACUS (T. Helgaker, H. J. Aa. Jensen, P. Jørgensen, and J. Olsen), and ECP routines by A. V. Mitin and C. van Wüllen. For the current version, see http://www.cfour.de.

(6) Aidas, K.; Angeli, C.; Bak, K. L.; Bakken, V.; Bast, R.; Boman, L.; Christiansen, O.; Cimiraglia, R.; Coriani, S.; Dahle, P. et al. The Dalton Quantum Chemistry Program System. *Wiley Interdiscip. Rev. Comput. Mol. Sci.* **2014**, *4*, 269–284.

(7) Dalton, a molecular electronic structure program. Release DALTON2013, 2014; see http://daltonprogram.org.

(8) Schmidt, M. W.; Baldridge, K. K.; Boatz, J. A.; Elbert, S. T.; Gordon, M. S.; Jensen, J. H.; Koseki, S.; Matsunaga, N.; Nguyen, K. A.; Su, S. et al. General Atomic and Molecular Electronic Structure System. *J. Comput. Chem.* **1993**, *14*, 1347–1363.

(9) Gordon, M. S.; Schmidt, M. W. In *Theory and Applications of Computational Chemistry: the First Forty Years*; Dykstra, C. E., Frenking, G., Kim, K. S., Scuseria, G., Eds.; Elsevier, 2005; Chapter Advances in electronic structure theory: GAMESS a decade later, pp 1167–1189.

(10) Frisch, M. J.; Trucks, G. W.; Schlegel, H. B.; Scuseria, G. E.; Robb, M. A.; Cheeseman, J. R.; Scalmani, G.; Barone, V.; Mennucci, B.; Petersson, G. A. et al. Gaussian 09 Revision D.01. Gaussian Inc. Wallingford CT 2009.

(11) Carter, S.; Sharma, A. R.; Bowman, J. M.; Rosmus, P.; Tarroni, R. Calculations of Rovibrational Energies and Dipole Transition Intensities for Polyatomic Molecules Using MULTIMODE. *J. Chem. Phys.* **2009**, *131*, 224106.

(12) Werner, H.-J.; Knowles, P. J.; Knizia, G.; Manby, F. R.; Schütz, M.; Celani, P.; Korona, T.; Lindh, R.; Mitrushenkov, A.; Rauhut, G. et al. MOLPRO, version 2012.1, a Package of ab initio Programs. 2012; see http://www.molpro.net.

(13) Valiev, M.; Bylaska, E. J.; Govind, N.; Kowalski, K.; Straatsma, T. P.; Van Dam, H. J. J.; Wang, D.; Nieplocha, J.; Apra, E.; Windus, T. L. et al. NWChem: A Comprehensive and Scalable Open-Source Solution for Large Scale Molecular Simulations. *Comput. Phys. Commun.* **2010**, *181*, 1477–1489.

(14) Shao, Y.; Molnar, L. F.; Jung, Y.; Kussmann, J.; Ochsenfeld, C.; Brown, S. T.; Gilbert, A. T.; Slipchenko, L. V.; Levchenko, S. V.; O'Neill, D. P. et al. Advances in Methods and Algorithms in a Modern Quantum Chemistry Program Package. *Phys. Chem. Chem. Phys.* **2006**, *8*, 3172–3191.

(15) Gaw, F.; Willetts, A.; Handy, N.; Green, W. In *Advances in Molecular Vibrations and Collision Dynamics*; Bowman, J. M., Ed.; JAI Press, 1992; Vol. 1; Chapter SPECTRO - a Program for Derivation of Spectroscopic Constants From Provided Quartic Force Fields and Cubic Dipole Fields.

(16) Carbonnière, P.; Dargelos, A.; Pouchan, C. The VCI-P Code: an Iterative Variation-Perturbation Scheme for Efficient Computations of Anharmonic Vibrational Levels and IR Intensities of Polyatomic Molecules. *Theor. Chem. Acc.* **2010**, *125*, 543–554.

(17) Carter, S.; Culik, S. J.; Bowman, J. M. Vibrational Self-Consistent Field Method for Many-Mode Systems: A New Approach and Application to the Vibrations of CO Adsorbed on Cu(100). *J. Chem. Phys.* **1997**, *107*, 10548–10469.

(18) Koput, J.; Carter, S.; Handy, N. C. Ab initio Prediction of The Vibrational-Rotational Energy Levels of Hydrogen Peroxide and its Isotopomers. *J. Chem. Phys.* **2001**, *115*, 8345–8350.

(19) Cassam-Chenaï, P.; Liévin, J. Alternative Perturbation Method for the Molecular Vibration-Rotation Problem. *Int. J. Quantum Chem.* **2003**, *93*, 245–264.

(20) Carrington, T.; Wang, X.-G. Computing Ro-Vibrational Spectra of Van Der Waals Molecules. *Wiley Interdiscip. Rev. Comput. Mol. Sci.* **2011**, *1*, 952–963.

(21) Tennyson, J. Accurate Variational Calculations for Line Lists to Model the Vibration–Rotation Spectra of Hot Astrophysical Atmospheres. *Wiley Interdiscip. Rev. Comput. Mol. Sci.* **2011**,

(22) Császár, A. G.; Fábri, C.; Szidarovszky, T.; Mátyus, E.; Furtenbacher, T.; Czakó, G. The Fourth Age of Quantum Chemistry: Molecules in Motion. *Phys. Chem. Chem. Phys.* **2012**, *14*, 1085–1106.

(23) Bowman, J. M. The Self-Consistent-Field Approach to Polyatomic Vibrations. *Acc. Chem. Res.* **1986**, *19*, 202–208.

(24) Chaban, G. M.; Jung, J. O.; Gerber, R. B. ab initio Calculation of Anharmonic Vibrational States of Polyatomic Systems: Electronic Structure Combined with Vibrational Self-Consistent Field. *J. Chem. Phys.* **1999**, *111*, 1823–1829.

(25) Wright, N. J.; Gerber, R. B. Direct Calculation of Anharmonic Vibrational States of Polyatomic Molecules Using Potential Energy Surfaces Calculated From Density Functional Theory. *J. Chem. Phys.* **2000**, *112*, 2598–2604.

(26) Gregurick, S. K.; Chaban, G. M.; Gerber, R. B. Ab initio and Improved Empirical Potentials for the Calculation of the Anharmonic Vibrational States and Intramolecular Mode Coupling of N-Methylacetamide. *J. Phys. Chem. A* **2002**, *106*, 8696–8707.

(27) Yagi, K.; Hirao, K.; Taketsugu, T.; Schmidt, M. W.; Gordon, M. S. Ab initio Vibrational State Calculations With a Quartic Force Field: Applications to H_2CO, C_2H_4, CH_3OH, CH_3CCH, and C_6H_6. *J. Chem. Phys.* **2004**, *121*, 1383–1389.

(28) Christiansen, O. Vibrational Structure Theory: New Vibrational Wave Function Methods for Calculation of Anharmonic Vibrational Energies and Vibrational Contributions to Molecular Properties. *Phys. Chem. Chem. Phys.* **2007**, *9*, 2942–2953.

(29) Rauhut, G.; Hrenar, T. A Combined Variational and Perturbational Study on the Vibrational Spectrum of P_2F_4. *Chem. Phys.* **2008**, *346*, 160–166.

(30) Christiansen, O. Selected New Developments in Vibrational Structure Theory: Potential Construction and Vibrational Wave Function Calculations. *Phys. Chem. Chem. Phys.* **2012**, *14*, 6672–6687.

(31) Roy, T. K.; Gerber, R. B. Vibrational Self-Consistent Field Calculations for Spec-

troscopy of Biological Molecules: New Algorithmic Developments and Applications. *Phys. Chem. Chem. Phys.* **2013**, *15*, 9468–9492.

(32) Nielsen, H. H. The Vibration-Rotation Energies of Molecules. *Rev. Mod. Phys.* **1951**, *23*, 90–136.

(33) Mills, I. M. In *Molecular Spectroscopy: Modern Research*; Rao, K. N., Mathews, C. W., Eds.; Academic Press, New York, 1972; Chapter Vibration-Rotation Structure in Asymmetric- and Symmetric-Top Molecules, pp 115–140.

(34) Hoy, A.; Mills, I.; Strey, G. Anharmonic Force Constant Calculations. *Mol. Phys.* **1972**, *24*, 1265–1290.

(35) Clabo Jr., D. A.; Allen, W. D.; Remington, R. B.; Yamaguchi, Y.; Schaefer III, H. F. A Systematic Study of Molecular Vibrational Anharmonicity and Vibration-Rotation Interaction by Self-Consistent-field Higher-Derivative Methods. Asymmetric Top Molecules. *Chem. Phys.* **1988**, *123*, 187–239.

(36) Schneider, W.; Thiel, W. Anharmonic Force Fields From Analytic Second Derivatives: Method and Application to Methyl Bromide. *Chem. Phys. Lett.* **1989**, *157*, 367–373.

(37) Allen, W. D.; Yamaguchi, Y.; Császár, A. G.; Clabo Jr., D. A.; Remington, R. B.; Schaefer III, H. F. A Systematic Study of Molecular Vibrational Anharmonicity and Vibration-Rotation Interaction by Self-Consistent-Field Higher-derivative Methods. Linear Polyatomic Molecules. *Chem. Phys.* **1990**, *145*, 427–466.

(38) Willets, A.; Handy, N. C.; Green, W. H., Jr.; Jayatilaka, D. Anharmonic Corrections to Vibrational Transition Intensities. *J. Phys. Chem.* **1990**, *94*, 5608–5616.

(39) Dressler, S.; Thiel, W. Anharmonic Force Fields From Density Functional Theory. *Chem. Phys. Lett.* **1997**, *273*, 71–78.

(40) Yagi, K.; Taketsugu, T.; Hirao, K.; Gordon, M. S. Direct Vibrational Self-Consistent Field Method: Applications to H_2O and H_2CO. *J. Chem. Phys.* **2000**, *113*, 1005–1017.

(41) Christiansen, O. Møller-Plesset Perturbation Theory for Vibrational Wave Functions. *J. Chem. Phys.* **2003**, *119*, 5773–5781.

(42) Neugebauer, J.; Hess, B. A. Fundamental Vibrational Frequencies of Small Polyatomic Molecules From Density-Functional Calculations and Vibrational Perturbation Theory. *J. Chem. Phys.* **2003**, *118*, 7215–7225.

(43) Ruden, T. A.; Taylor, P. R.; Helgaker, T. Automated Calculation of Fundamental Frequencies: Application to AlH_3 Using the Coupled-Cluster Singles-and-Doubles With Perturbative Triples Method. *J. Chem. Phys.* **2003**, *119*, 1951–1960.

(44) Krasnoshchekov, S. V.; Isayeva, E. V.; Stepanov, N. F. Numerical-Analytic Implementation of the Higher-Order Canonical Van Vleck Perturbation Theory for the Interpretation of Medium-Sized Molecule Vibrational Spectra. *J. Phys. Chem. A* **2012**, *116*, 3691–3709.

(45) Barone, V. Anharmonic Vibrational Properties by a Fully Automated Second-Order Perturbative Approach. *J. Chem. Phys.* **2005**, *122*, 014108.

(46) Császár, A. G. Anharmonic Molecular Force Fields. *Wiley Interdiscip. Rev. Comput. Mol. Sci.* **2011**,

(47) Gaw, J. F.; Yamaguchi, Y.; Schaefer, H. F.; Handy, N. C. Generalization of Analytic Energy Third Derivatives for the RHF Closed–Shell Wave Function: Derivative Energy and Integral Formalisms and the Prediction of Vibration–Rotation Interaction Constants. *J. Chem. Phys.* **1986**, *85*, 5132–5142.

(48) Colwell, S. M.; Jayatilaka, D.; Maslen, P. E.; Amos, R. D.; Handy, N. C. Higher

Analytic Derivatives. I. A New Implementation for the Third Derivative of the SCF Energy. *Int. J. Quantum Chem.* **1991**, *40*, 179–199.

(49) Maslen, P. E.; Jayatilaka, D.; Colwell, S. M.; Amos, R. D.; Handy, N. C. Higher Analytic Derivatives. II. The Fourth Derivative of Self-Consistent-Field Energy. *J. Chem. Phys.* **1991**, *95*, 7409–7417.

(50) Ringholm, M.; Jonsson, D.; Bast, R.; Gao, B.; Thorvaldsen, A. J.; Ekstrm, U.; Helgaker, T.; Ruud, K. Analytic Cubic and Quartic Force Fields Using Density-Functional Theory. *J. Chem. Phys.* **2014**, *140*, 034103.

(51) Vázquez, J.; Stanton, J. F. Simple(r) Algebraic Equation for Transition Moments of Fundamental Transitions in Vibrational Second-Order Perturbation Theory. *Mol. Phys.* **2006**, *104*, 377–388.

(52) Maslen, P. E.; Handy, N. C.; Amos, R. D.; Jayatilaka, D. Higher Analytic Derivatives. IV. Anharmonic Effects in the Benzene Spectrum. *J. Chem. Phys.* **1992**, *97*, 4233–4254.

(53) Montero, S. Anharmonic Raman Intensities of Overtones, Combination and Difference Bands. *J. Chem. Phys.* **1982**, *77*, 23–29.

(54) Faulkner, T. R.; Marcott, C.; Moscowitz, A.; Overend, J. Anharmonic Effects in Vibrational Circular Dichroism. *J. Am. Chem. Soc.* **1977**, *99*, 8160–8168.

(55) Bouř, P. Anharmonic Corrections to Vibrational Energies of Molecules: Water and Dideuteriooxirane. *J. Phys. Chem.* **1994**, *98*, 8862–8865.

(56) Miller, W. H.; Hernandez, R.; Handy, N. C.; Jayatilaka, D.; Willets, A. Ab Initio Calculation of Anharmonic Constants for a Transition State, With Application to Semiclassical Transition State Tunneling Probabilities. *Chem. Phys. Lett.* **1990**, *172*, 62–68.

(57) Vázquez, J.; Stanton, J. F. Treatment of Fermi Resonance Effects on Transition Moments in Vibrational Perturbation Theory. *Mol. Phys.* **2007**, *105*, 101–109.

(58) Bloino, J.; Barone, V. A Second-Order Perturbation Theory Route to Vibrational Averages and Transition Properties of Molecules: General Formulation and Application to Infrared and Vibrational Circular Dichroism Spectroscopies. *J. Chem. Phys.* **2012**, *136*, 124108.

(59) Cappelli, C.; Bloino, J.; Lipparini, F.; Barone, V. Toward Ab initio Anharmonic Vibrational Circular Dichroism Spectra in the Condensed Phase. *J. Phys. Chem. Lett.* **2012**, *3*, 1766–1773.

(60) Egidi, F.; Bloino, J.; Cappelli, C.; Barone, V. Development of a Virtual Spectrometer for Chiroptical Spectroscopies: The Case of Nicotine. *Chirality* **2013**, *25*, 701–708.

(61) Merten, C.; Bloino, J.; Barone, V.; Xu, Y. Anharmonicity Effects in the Vibrational CD Spectra of Propylene Oxide. *J. Phys. Chem. Lett.* **2013**, *4*, 3424–3428.

(62) Barone, V.; Biczysko, M.; Bloino, J. Fully Anharmonic IR and Raman Spectra of Medium-Size Molecular Systems: Accuracy and Interpretation. *Phys. Chem. Chem. Phys.* **2014**, *16*, 1759–1787.

(63) Martin, J. M. L.; Lee, T. J.; Taylor, P. M.; François, J.-P. The Anharmonic Force Field of Ethylene, C_2H_4, by Means of Accurate Ab Initio Calculations. *J. Chem. Phys.* **1995**, *103*, 2589–2602.

(64) Kuhler, K. M.; Truhlar, D. G.; Isaacson, A. D. General Method for Removing Resonance Singularities in Quantum Mechanical Perturbation Theory. *J. Chem. Phys.* **1996**, *104*, 4664–4670.

(65) Bloino, J.; Biczysko, M.; Barone, V. General Perturbative Approach for Spectroscopy,

Thermodynamics, and Kinetics: Methodological Background and Benchmark Studies. *J. Chem. Theory Comput.* **2012**, *8*, 1015–1036.

(66) Rosnik, A. M.; Polik, W. F. VPT2+K Spectroscopic Constants and Matrix Elements of the Transformed Vibrational Hamiltonian of a Polyatomic Molecule With Resonances Using Van Vleck Perturbation Theory. *Mol. Phys.* **2014**, *112*, 261–300.

(67) Cheeseman, J. R.; Frisch, M. J.; Devlin, F. J.; Stephens, P. J. Ab initio Calculation of Atomic Axial Tensors and Vibrational Rotational Strengths Using Density Functional Theory. *Chem. Phys. Lett.* **1996**, *252*, 211–220.

(68) Stephens, P. J. Theory of Vibrational Circular Dichroism. *J. Phys. Chem.* **1985**, *89*, 748–752.

(69) Bak, K. L.; Bludský, O.; Jørgensen, P. *Ab initio* Calculations of Anharmonic Vibrational Circular Dichroism Intensities of *trans*-2,3-dideuteriooxirane. *J. Chem. Phys.* **1995**, *103*, 10548–10555.

(70) Barone, V.; Cimino, P. Accurate and Feasible Computations of Structural and Magnetic Properties of Large Free Radicals: The PBE0/N07D Model. *Chem. Phys. Lett.* **2008**, *454*, 139–143.

(71) Barone, V.; Cimino, P.; Stendardo, E. Development and Validation of the B3LYP/N07D Computational Model for Structural Parameter and Magnetic Tensors of Large Free Radicals. *J. Chem. Theory Comput.* **2008**, *4*, 751–764.

(72) Barone, V.; Cimino, P. Validation of the B3LYP/N07D and PBE0/N07D Computational Models for the Calculation of Electronic g-Tensors. *J. Chem. Theory Comput.* **2009**, *5*, 192–199.

(73) Barone, V.; Biczysko, M.; Bloino, J.; Borkowska-Panek, M.; Carnimeo, I.; Panek, P.

Toward Anharmonic Computations of Vibrational Spectra for Large Molecular Systems. *Int. J. Quantum Chem.* **2012**, *112*, 2185–2200.

(74) Swofford, R. L.; Long, M. E.; Albrecht, A. C. C-H Vibrational States of Benzene, Naphthalene, and Anthracene in the Visible Region by Thermal Lensing Spectroscopy and the Local Mode Model. *J. Chem. Phys.* **1976**, *65*, 179–190.

(75) Burberry, M. S.; Morrell, J. A.; Albrecht, A. C.; Swofford, R. L. Local Mode Overtone Intensities of C-H Stretching Modes in Alkanes and Methyl Substituted Benzenes. *J. Chem. Phys.* **1979**, *70*, 5522–5526.

(76) Wong, J. S.; Moore, C. B. Inequivalent C-H Oscillators of Gaseous Alkanes and Alkenes in Laser Photoacoustic Overtone Spectroscopy. *J. Chem. Phys.* **1982**, *77*, 603–615.

(77) Fang, H. L.; Compton, D. A. C. Overtone Spectroscopy of Nonequivalent Carbon-Hydrogen Oscillators in 1-Alkenes and Dienes. *J. Phys. Chem.* **1988**, *92*, 7185–7192.

(78) Hudgins, D. M.; Sandford, S. A.; Allamandola, L. J. Infrared Spectroscopy of Polycyclic Aromatic Hydrocarbon Cations. 1. Matrix-Isolated Naphthalene and Perdeuterated Naphthalene. *J. Phys. Chem.* **1994**, *98*, 4243–4253, PMID: 12269375.

(79) Kjaergaard, H. G.; Henry, B. R. CH Stretching Overtone Spectra and Intensities of Vapor Phase Naphthalene. *J. Phys. Chem.* **1995**, *99*, 899–904.

(80) Lopez-Calvo, A.; Diez-y Riega, H.; Manzanares, C. E. Vibrational C-H overtone Spectroscopy and Bond Distances of Butenes Dissolved in Liquid Xe. *J. Mol. Struct.* **2009**, *935*, 39–46.

(81) Burcl, R.; Carter, S.; Handy, N. C. On the Representation of Potential Energy Surfaces of Polyatomic Molecules in Normal Coordinates: II. Parameterisation of the Force Field. *Chem. Phys. Lett.* **2003**, *373*, 357–365.

(82) Konen, I. M.; Pollack, I. B.; Li, E. X. J.; Lester, M. I.; Varner, M. E.; Stanton, J. F. Infrared Overtone Spectroscopy and Unimolecular Decay Dynamics of Peroxynitrous Acid. *J. Chem. Phys.* **2005**, *122*, 094320.

(83) Perrin, A. Recent Progress in the Analysis of HNO_3 Spectra. *Spectrochim. Acta A Mol. Biomol. Spectrosc.* **1998**, *54*, 375–393.

(84) Feierabend, K. J.; Havey, D. K.; Varner, M. E.; Stanton, J. F.; Vaida, V. A Comparison of Experimental and Calculated Spectra of HNO3 in the Near-Infrared Using Fourier transform Infrared Spectroscopy and Vibrational Perturbation Theory. *J. Chem. Phys.* **2006**, *124*, 124323.

(85) Raghavachari, K.; Trucks, G. W.; Pople, J. A.; Head-Gordon, M. A Fifth-Order Perturbation Comparison of Electron Correlation Theories. *Chem. Phys. Lett.* **1989**, *157*, 479–483.

(86) Almlöf, J.; Taylor, P. R. General Contraction of Gaussian Basis Sets. I. Atomic Natural Orbitals for First- and Second-row Atoms. *J. Chem. Phys.* **1987**, *86*, 4070–4077.

(87) Begue, D.; Carbonniere, P.; Pouchan, C. Calculations of Vibrational Energy Levels by Using a Hybrid ab initio and DFT Quartic Force Field: Application to Acetonitrile. *J. Phys. Chem. A* **2005**, *109*, 4611–4616, PMID: 16833799.

(88) Puzzarini, C.; Biczysko, M.; Barone, V. Accurate Harmonic/Anharmonic Vibrational Frequencies for Open-Shell Systems: Performances of the B3LYP/N07D Model for Semirigid Free Radicals Benchmarked by CCSD(T) Computations. *J. Chem. Theory Comput.* **2010**, *6*, 828–838.

(89) Puzzarini, C.; Biczysko, M.; Barone, V. Accurate Anharmonic Vibrational Frequencies for Uracil: The Performance of Composite Schemes and Hybrid CC/DFT Model. *J. Chem. Theory Comput.* **2011**, *7*, 3702–3710.

(90) Biczysko, M.; Bloino, J.; Brancato, G.; Cacelli, I.; Cappelli, C.; Ferretti, A.; Lami, A.; Monti, S.; Pedone, A.; Prampolini, G. et al. Integrated Computational Approaches for Spectroscopic Studies of Molecular Systems in the Gas Phase and in Solution: Pyrimidine as a Test Case. *Theor. Chem. Acc.* **2012**, *131*, 1–19.

(91) Barone, V.; Biczysko, M.; Bloino, J.; Egidi, F.; Puzzarini, C. Accurate Structure, Thermodynamics, and Spectroscopy of Medium-sized Radicals by Hybrid Coupled Cluster/Density Functional Theory Approaches: The Case of Phenyl Radical. *J. Chem. Phys.* **2013**, *138*, 234303.

(92) Barone, V.; Biczysko, M.; Bloino, J.; Puzzarini, C. Glycine Conformers: a Never-Ending Story? *Phys. Chem. Chem. Phys.* **2013**, *15*, 1358–1363.

(93) Barone, V.; Biczysko, M.; Bloino, J.; Puzzarini, C. Accurate Structure, Thermodynamic and Spectroscopic Parameters From CC and CC/DFT Schemes: the Challenge of the Conformational Equilibrium in Glycine. *Phys. Chem. Chem. Phys.* **2013**, *15*, 10094–10111.

(94) Barone, V.; Biczysko, M.; Bloino, J.; Puzzarini, C. Characterization of the Elusive Conformers of Glycine from State-of-the-Art Structural, Thermodynamic, and Spectroscopic Computations: Theory Complements Experiment. *J. Chem. Theory Comput.* **2013**, *9*, 1533–1547.

(95) Charmet, A. P.; Stoppa, P.; Tasinato, N.; Giorgianni, S.; Barone, V.; Biczysko, M.; Bloino, J.; Cappelli, C.; Carnimeo, I.; Puzzarini, C. An Integrated Experimental and Quantum-Chemical Investigation on the Vibrational Spectra of Chlorofluoromethane. *J. Chem. Phys.* **2013**, *139*, 164302.

(96) Puzzarini, C.; Biczysko, M.; Bloino, J.; Barone, V. Accurate Spectroscopic Characterization of Oxirane: A Valuable Route to its Identification in Titan's Atmosphere and the Assignment of Unidentified Infrared Bands. *Astrophys. J.* **2014**, *785*, 107.

(97) Feierabend, K. J.; Havey, D. K.; Vaida, V. Gas Phase Spectroscopy of HNO_3 in the Region 2000–8500 cm^{-1}. *Spectrochim. Acta A Mol. Biomol. Spectrosc.* **2004**, *60*, 2775–2781.

(98) Tielens, A. Interstellar Polycyclic Aromatic Hydrocarbon Molecules. *Annu. Rev. Astron. Astrophys.* **2008**, *46*, 289–337.

(99) Kwok, S.; Zhang, Y. Mixed Aromatic-Aliphatic Organic Nanoparticles as Carriers of Unidentified Infrared Emission Features. *Nature* **2011**, *479*, 80–83.

(100) Lippincott, E. R.; O'Reilly, E. J. Vibrational Spectra and Assignment of Naphthalene and Naphthalene-d-8. *J. Chem. Phys.* **1955**, *23*, 238–244.

(101) Ferguson, J.; Reeves, L. W.; Schneider, W. G. Vapor Absorption Spectra and Oscillator Strengths of Naphthalene, Anthracene, and Pyrene. *Can. J. Chem.* **1957**, *35*, 1117–1136.

(102) Cané, E.; Miani, A.; Trombetti, A. Anharmonic Force Fields of Naphthalene-h8 and Naphthalene-d8. *J. Phys. Chem. A* **2007**, *111*, 8218–8222.

(103) Pirali, O.; Vervloet, M.; Mulas, G.; Malloci, G.; Joblin, C. High-resolution Infrared Absorption Spectroscopy of Thermally Excited Naphthalene. Measurements and Calculations of Anharmonic Parameters and Vibrational Interactions. *Phys. Chem. Chem. Phys.* **2009**, *11*, 3443–3454.

(104) Albert, S.; Albert, K. K.; Lerch, P.; Quack, M. Synchrotron-based Highest Resolution Fourier Transform Infrared Spectroscopy of Naphthalene ($C_{10}H_8$) and Indole (C_8H_7N) and its Application to Astrophysical Problems. *Faraday Discuss.* **2011**, *150*, 71–99.

(105) Pirali, O.; Goubet, M.; Huet, T. R.; Georges, R.; Soulard, P.; Asselin, P.; Courbe, J.; Roy, P.; Vervloet, M. The Far Infrared Spectrum of Naphthalene Characterized by

High Resolution Synchrotron FTIR Spectroscopy and Anharmonic DFT Calculations. *Phys. Chem. Chem. Phys.* **2013**, *15*, 10141–10150.

(106) NIST Mass Spec Data Center, S.E. Stein, director, In *NIST Chemistry WebBook, NIST Standard Reference Database Number 69*; Linstrom, P. J., Mallard, W. G., Eds.; National Institute of Standards and Technology: Gaithersburg MD, 20899, Chapter Infrared Spectra, http://webbook.nist.gov, (retrieved September 20, 2014).

(107) Pathak, C. M.; Fletcher, W. H. Infrared and Raman Spectra of Isobutene and Isobutene-d_8. *J. Mol. Spectrosc.* **1969**, *31*, 32–53.

(108) Guo, H.; Karplus, M. Basis Set and Polarization Function Effects on Optimized Geometries and Harmonic Frequencies at the Second–Order Møller–Plesset Perturbation Level. *J. Chem. Phys.* **1989**, *91*, 1719–1733.

(109) Mannfors, B.; Sundius, T.; Palmo, K.; Pietila, L.-O.; Krimm, S. Spectroscopically Determined Force Fields for Macromolecules. Part 3. Alkene Chains. *J. Mol. Struct.* **2000**, *521*, 49–75.

(110) Lopez-Calvo, A. Vibrational Spectroscopy in Cryogenic Solutions: Application of Thermal Lensing and Fourier Transform Techniques to the Study of Molecular C-H Overtone Transitions. Ph.D. thesis, Baylor University, 2006.

(111) Cancès, E.; Mennucci, B.; Tomasi, J. A New Integral Equation Formalism for the Polarizable Continuum Model: Theoretical Background and Applications to Isotropic and Anisotropic Dielectrics. *J. Chem. Phys.* **1997**, *107*, 3032–3041.

(112) Tomasi, J.; Mennucci, B.; Cammi, R. Quantum Mechanical Continuum Solvation Models. *Chem. Rev.* **2005**, *105*, 2999–3094.

Graphical TOC Entry